



Recent Development in the CESE Method for the Solution of the Navier-Stokes Equations Using Unstructured Triangular or Tetrahedral Meshes With High Aspect Ratio

Sin-Chung Chang
Glenn Research Center, Cleveland, Ohio

Chau-Lyan Chang
Langley Research Center, Hampton, Virginia

Joseph C. Yen
Jacobs Technology Inc., Tullahoma, Tennessee

NASA STI Program . . . in Profile

Since its founding, NASA has been dedicated to the advancement of aeronautics and space science. The NASA Scientific and Technical Information (STI) program plays a key part in helping NASA maintain this important role.

The NASA STI Program operates under the auspices of the Agency Chief Information Officer. It collects, organizes, provides for archiving, and disseminates NASA's STI. The NASA STI program provides access to the NASA Aeronautics and Space Database and its public interface, the NASA Technical Reports Server, thus providing one of the largest collections of aeronautical and space science STI in the world. Results are published in both non-NASA channels and by NASA in the NASA STI Report Series, which includes the following report types:

- **TECHNICAL PUBLICATION.** Reports of completed research or a major significant phase of research that present the results of NASA programs and include extensive data or theoretical analysis. Includes compilations of significant scientific and technical data and information deemed to be of continuing reference value. NASA counterpart of peer-reviewed formal professional papers but has less stringent limitations on manuscript length and extent of graphic presentations.
- **TECHNICAL MEMORANDUM.** Scientific and technical findings that are preliminary or of specialized interest, e.g., quick release reports, working papers, and bibliographies that contain minimal annotation. Does not contain extensive analysis.
- **CONTRACTOR REPORT.** Scientific and technical findings by NASA-sponsored contractors and grantees.

- **CONFERENCE PUBLICATION.** Collected papers from scientific and technical conferences, symposia, seminars, or other meetings sponsored or cosponsored by NASA.
- **SPECIAL PUBLICATION.** Scientific, technical, or historical information from NASA programs, projects, and missions, often concerned with subjects having substantial public interest.
- **TECHNICAL TRANSLATION.** English-language translations of foreign scientific and technical material pertinent to NASA's mission.

Specialized services also include creating custom thesauri, building customized databases, organizing and publishing research results.

For more information about the NASA STI program, see the following:

- Access the NASA STI program home page at <http://www.sti.nasa.gov>
- E-mail your question to help@sti.nasa.gov
- Fax your question to the NASA STI Information Desk at 443-757-5803
- Phone the NASA STI Information Desk at 443-757-5802
- Write to:
STI Information Desk
NASA Center for AeroSpace Information
7115 Standard Drive
Hanover, MD 21076-1320



Recent Development in the CESE Method for the Solution of the Navier-Stokes Equations Using Unstructured Triangular or Tetrahedral Meshes With High Aspect Ratio

Sin-Chung Chang
Glenn Research Center, Cleveland, Ohio

Chau-Lyan Chang
Langley Research Center, Hampton, Virginia

Joseph C. Yen
Jacobs Technology Inc., Tullahoma, Tennessee

Prepared for the
21st Computational Fluid Dynamics Conference
sponsored by the American Institute of Aeronautics and Astronautics
San Diego, California, June 24–27, 2013

National Aeronautics and
Space Administration

Glenn Research Center
Cleveland, Ohio 44135

Acknowledgments

Sin-Chung Chang would like to express his deep gratitude to Dr. Grant Cook, a friend and teacher, for his encouragement during the course of the CESE development.

This work was sponsored by the Fundamental Aeronautics Program
at the NASA Glenn Research Center.

Level of Review: This material has been technically reviewed by technical management.

Available from

NASA Center for Aerospace Information
7115 Standard Drive
Hanover, MD 21076-1320

National Technical Information Service
5301 Shawnee Road
Alexandria, VA 22312

Available electronically at <http://www.sti.nasa.gov>

Recent Development in the CESE Method for the Solution of the Navier-Stokes Equations Using Unstructured Triangular or Tetrahedral Meshes With High Aspect Ratio

Sin-Chung Chang
National Aeronautics and Space Administration
Glenn Research Center
Cleveland, Ohio 44135

Chau-Lyan Chang
National Aeronautics and Space Administration
Langley Research Center
Hampton, Virginia 23681

Joseph C. Yen
Jacobs Technology Inc.
Tullahoma, Tennessee 37388

Abstract

In the multidimensional CESE development, triangles and tetrahedra turn out to be the most natural building blocks for 2D and 3D spatial meshes. As such the CESE method is compatible with the simplest unstructured meshes and thus can be easily applied to solve problems with complex geometries. However, because the method uses space-time staggered stencils, solution decoupling may become a real nuisance in applications involving unstructured meshes. In this paper we will describe a simple and general remedy which, according to numerical experiments, has removed any possibility of solution decoupling. Moreover, in a real-world viscous flow simulation near a solid wall, one often encounters a case where a boundary with high curvature or sharp corner is surrounded by triangular/tetrahedral meshes of extremely high aspect ratio (up to 10^6). For such an extreme case, the spatial projection of a space-time compounded conservation element constructed using the original CESE design may become highly concave and thus its centroid (referred to as a spatial solution point) may lie far outside of the spatial projection. It could even be embedded beyond a solid wall boundary and causes serious numerical difficulties. In this paper we will also present a new procedure for constructing conservation elements and solution elements which effectively overcomes the difficulties associated with the original design. Another difficulty issue which was addressed more recently is the well-known fact that accuracy of gradient computations involving triangular/tetrahedral grids deteriorates rapidly as the aspect ratio of grid cells increases. The root cause of this difficulty was clearly identified and several remedies to overcome it were found through a rigorous mathematical analysis. However, because of the length of the current paper and the complexity of mathematics involved, this new work will be presented in another paper.

1. Introduction

The space-time conservation element and solution element (CESE) method is a high-resolution and genuinely multidimensional method for solving conservation laws [1–70]. Its nontraditional features include: (i) a unified treatment of space and time; (ii) the introduction of conservation elements (CEs) and solution elements (SEs) as the vehicles for enforcing space-time flux conservation; (iii) a time marching strategy that has a space-time staggered stencil at its core and, as such, fluxes at an interface can be evaluated without using

any interpolation or extrapolation procedure (which, in turn, leads to the method’s ability to capture shocks without using Riemann solvers, and also partially contributes to the unusually simple CESE non-reflecting boundary conditions); (iv) the requirement that each scheme be built from a nondissipative core scheme and, as a result, the numerical dissipation can be controlled effectively; and (v) the fact that mesh values of the physical dependent variables and their spatial derivatives are considered as independent mesh variables to be solve for simultaneously. Note that CEs are non-overlapping space-time subdomains introduced such that (i) the computational domain can be filled by these subdomains; and (ii) flux conservation can be enforced over each of them and also over the union of any combination of them. On the other hand, SEs are space-time subdomains introduced such that (i) the boundary of each CE can be divided into component parts with each of them belonging to a unique SE; and (ii) within a SE, any physical flux vector is approximated using simple smooth functions constructed from the solution information stored at a space-time solution point. In general, a CE does not coincide with a SE.

Without using flux-splitting, dimensional-splitting, mesh-alignment or other special techniques, since its inception in 1991 [1], the unstructured-mesh compatible 2nd-order CESE method has been used to obtain numerous accurate 1D, 2D and 3D steady and unsteady flow solutions with Mach numbers ranging from 0.0028 to 10 [15]. The physical phenomena modeled include traveling and interacting shocks, acoustic waves, vortex shedding, viscous flows, detonation waves, cavitation, flows in fluid film bearings, heat conduction with melting and/or freezing, MHD vortex, hydraulic jump, crystal growth, chromatographic problems, solar wind and stress waves in elastic solids [3–70]. In particular, its unexpected simple non-reflecting boundary conditions [12,50] and rather unique capability to resolve both strong shocks and small disturbances (e.g., acoustic waves) simultaneously [19,21,22,66,67] make the CESE method an effective tool for attacking computational aeroacoustics (CAA) problems. Note that the fact that the second-order CESE method is capable of solving CAA problems accurately is an exception to the commonly-held belief that a second-order scheme is not adequate for modeling CAA problems. Also note that, while numerical dissipation is needed for shock capturing, it may also result in annihilation of small disturbances. Thus a solver that can handle both strong shocks and small disturbances simultaneously must be able to overcome this difficulty.

In spite of its nontraditional features and robust capabilities, the core ideas of the CESE method are simple. In fact, all of its key features are the results of a pursuit driven by these simple ideas. The first and foremost is the belief that the method must be solid in physics. As such, in the CESE development, conservation laws are enforced locally and globally in their natural space-time unity forms for 1D, 2D and 3D cases. Moreover, because *direct* physical interaction generally occurs only among the immediate neighbors, use of the simplest stencil also becomes a common CESE feature. Obviously, this requirement has the effect of simplifying boundary-condition implementation.

The second idea emerges from the realization that stability and accuracy are two competing issues in time-accurate computations, i.e., too much numerical dissipation will degrade accuracy while too little of it will cause instability. In other words, to meet both accuracy and stability requirements, computation must be performed away from the edge (“cliff”) of instability but not too far from it. This represents a real dilemma in numerical method development. As an example, high order schemes generally have higher accuracy and lower numerical dissipation. However, they are susceptible to computational instabilities. In fact, in complicated real-world applications, not only they seldom live up to their nominal order of accuracy—generally they possess only first-order accuracy when shocks are present, *stability of these schemes often is highly problem-dependent and difficulty to predict. Moreover, generally speaking, the higher the order of the scheme, the more restrictive its stability conditions become.* To confront this issue head-on, in the CESE development, generally it is required that a solver be built from a nondissipative (i.e., neutrally stable) core scheme. By definition, computations involving a neutrally stable scheme are performed right on the edge of instability and therefore the numerical results generated are nondissipative. As such numerical dissipation can be controlled effectively if the deviation of a solver from its nondissipative core scheme can be adjusted using some built-in parameters.

Moreover, because an accurate viscous flow simulation requires that the numerical dissipation be much smaller than the physical dissipation which decreases as the Reynolds number increases, *in principle, an accurate and robust solver for high-Reynolds-number flows must be able to cut numerical dissipation as the*

Reynolds number increases. Obviously this requirement can only be met by a solver built from a nondissipative core solver.

Other CESE ideas are: (i) the flux at an interface be evaluated in a simple and consistent manner; (ii) *genuinely* multidimensional schemes be built as simple, consistent and straightforward extensions of 1D schemes so that *multidimensional shocks can be captured without using any mesh alignment technique*; (iii) triangular and tetrahedral meshes be used in 2D and 3D cases, respectively, so that the method is compatible with the simplest unstructured meshes and thus can be easily used to solve problems with complex geometries; and (iv) logical structures and approximation techniques used be as simple as possible, and special techniques that has only limited applicability and may cause undesirable side effects be avoided. Fortunately for the CESE development, realization of the above lesser ideas (i)–(iv) follows naturally from the first two core ideas.

Building on its initial successes, efforts to refine and improve the CESE method have continued in the past few years. As an example, it was shown in [5] that the numerical dissipation of a dissipative extension of a CESE core scheme may increase to an intolerable level as the value of the *CFL* number decreases from its maximum stability bound. As such, in a case with a large *CFL* number disparity (e.g., a simulation with a highly non-uniform spatial mesh and a spatially independent time step), the performance sensitivity with respect to the *CFL* number can lead to a solution that is highly dissipative in a region where the local *CFL* number $\ll 1$. Even though a remedy was suggested in [5], a simple and robust solution to this problem had not arrived until a family of new Courant number insensitive schemes [25,31,46–49,51,54,55,58] was developed with fresh insights. Note that these new schemes have one important advantage, i.e., **all variables at each mesh point can be evaluated explicitly without resorting to solving a system of linear/nonlinear algebraic equations involving these local mesh variables even in applications where systems of multidimensional nonlinear PDEs are solved.**

As another example, even though they are accurate enough to solve CAA problems, second-order CESE solvers are not capable of resolving fine flow structures within a boundary layer without using relatively fine meshes and/or meshes with large aspect ratios. To overcome this limitation, two neutrally stable 4th-order schemes, referred to as the *a*(3) and *a*-4 schemes [59–61], were developed in 2006 and intended to serve as the core schemes of other high order CESE schemes. Unfortunately, the dissipative extensions of these new schemes turned out to have the same intractable stability problem that afflicts traditional high order schemes. With the aid of a conceptual leap, this difficulty was finally overcome through the development of a new approach [63] by which one can build from a given 2nd-order CESE scheme its 4th-, 6th-, 8th-,... order versions which **have the same stencil and same stability conditions of the 2nd-order scheme, and also retain all other advantages of the latter scheme.** As such, these new high order schemes can avoid the common shortcomings of traditional high order schemes including: (a) **susceptibility to computational instabilities**; (b) **computational inefficiency due to their local implicit nature (i.e., at each mesh points, need to solve a system of linear/nonlinear equations involving all the mesh variables associated with this mesh point)**; (c) **use of large and elaborate stencils which complicates boundary treatments and also makes efficient parallel computing much harder**; (d) **difficulties in applications involving complex geometries**; and (e) **use of problem-specific techniques which are needed to overcome stability problems but often cause undesirable side effects.**

In the current paper, we will describe other recent developments which successfully address some of the few remaining CESE issues. Some of the new techniques devised have been implemented in the NASA code ez4d (developed by Dr. Chau-Lyan Chang, the second author) and the Jacobs Technology Inc. code JUSTUS (developed by Dr. Joseph C. Yen, the third author). Their effectiveness has been verified by applications involving hypersonic viscous flow over rough solid surfaces [62,64,65] and also by applications involving studies of the WICS (weapons Internal Carriage and separation) test data produced at Arnold Engineering Development Center [66,67]. Note that the current paper would represent the first systematic documentation of the new techniques even though the improved numerical results were presented in [62,64–67]. To explain clearly these new techniques and their significance, we will begin our discussion by providing some basic information about the CESE method.

For simplicity, first we review existing 2nd-order CESE solvers for the simple partial differential equation (PDE)

$$\frac{\partial u}{\partial t} + a \frac{\partial u}{\partial x} = 0 \quad (1.1)$$

where the advection speed $a \neq 0$ is a constant. Let $x_1 = x$, and $x_2 = t$ be the coordinates of a two-dimensional Euclidean space E_2 . Then, because Eq. (1.1) can be expressed as $\vec{\nabla} \cdot \vec{h} = 0$ with $\vec{h} \stackrel{\text{def}}{=} (au, u)$ (i.e., au and u are the x_1 - and x_2 - components of \vec{h} , respectively), Gauss' divergence theorem in the space-time E_2 implies that Eq. (1.1) is the differential form of the integral conservation law

$$\oint_{S(V)} \vec{h} \cdot d\vec{s} = 0 \quad (1.2)$$

As depicted in Fig. 1, here (i) $S(V)$ is the boundary of an arbitrary *space-time* region V in E_2 , and (ii) $d\vec{s} = d\sigma \vec{n}$ with $d\sigma$ and \vec{n} , respectively, being the area and the unit outward normal vector of a surface element on $S(V)$. Note that: (i) because $\vec{h} \cdot d\vec{s}$ is the *space-time* flux of \vec{h} leaving the region V through the surface element $d\vec{s}$, Eq. (1.2) simply states that the total *space-time* flux of \vec{h} leaving V through $S(V)$ vanishes; (ii) in E_2 , $d\sigma$ is the length of a differential line segment on the simple closed curve $S(V)$; and (iii) all mathematical operations can be carried out as though E_2 were an ordinary two-dimensional Euclidean space.

To proceed, let Ω_1 denote the set of all space-time staggered mesh points (j, n) in E_2 (dots in Fig. 2(a)), where $n = 0, \pm 1/2, \pm 1, \pm 3/2, \pm 2, \dots$, and, for each n , $j = n \pm 1/2, n \pm 3/2, n \pm 5/2, \dots$. Thus $(j + n)$ is an half integer for each $(j, n) \in \Omega_1$. Each $(j, n) \in \Omega_1$ is associated with a solution element, i.e., $\text{SE}(j, n)$. By definition, $\text{SE}(j, n)$ is the *interior* of the *space-time* region bounded by a dashed curve depicted in Fig. 2(b). It includes a horizontal line segment, a vertical line segment, and their immediate neighborhood. By definition, the end points of the line segments referred to above are excluded from $\text{SE}(j, n)$ so that two SEs will not overlap.

Eq. (1.2) will be simulated numerically assuming that, for any $(x, t) \in \text{SE}(j, n)$, $u(x, t)$ and $\vec{h}(x, t)$, respectively, are approximated by

$$u^*(x, t; j, n) \stackrel{\text{def}}{=} u_j^n + (u_x)_j^n (x - x_j) + (u_t)_j^n (t - t^n) \quad (j, n) \in \Omega_1 \quad (1.3)$$

and

$$\vec{h}^*(x, t; j, n) \stackrel{\text{def}}{=} (au^*(x, t; j, n), u^*(x, t; j, n)) \quad (x, t) \in \text{SE}(j, n) \text{ and } (j, n) \in \Omega_1 \quad (1.4)$$

Note that: (i) u_j^n , $(u_x)_j^n$, and $(u_t)_j^n$ are constants in $\text{SE}(j, n)$, and (in a rough sense) they can be considered as the numerical analogues of the values of u , $\partial u / \partial x$, and $\partial u / \partial t$ at the mesh point (j, n) , respectively, (ii) (x_j, t^n) are the coordinates of the mesh point (j, n) with $x_j = j\Delta x$ and $t^n = n\Delta t$, and (iii) Eq. (1.4) is the numerical analogue of the definition $\vec{h} = (au, u)$.

Let $u = u^*(x, t; j, n)$ satisfy Eq. (1.1) within $\text{SE}(j, n)$. Then one has

$$(u_t)_j^n = -a (u_x)_j^n \quad (j, n) \in \Omega_1 \quad (1.5)$$

As a result, Eq. (1.3) reduces to

$$u^*(x, t; j, n) = u_j^n + (u_x)_j^n [(x - x_j) - a(t - t^n)] \quad (j, n) \in \Omega_1 \quad (1.6)$$

i.e., u_j^n and $(u_x)_j^n$ are the only independent mesh variables associated with (j, n) .

Let E_2 be divided into non-overlapping rectangular regions (see Fig. 2(a)) referred to as basic conservation elements (BCEs). As depicted in Figs. 2(c)–2(e), (i) each $(j, n) \in \Omega_1$ is assigned with two BCEs, i.e., $\text{CE}_-(j, n)$ and $\text{CE}_+(j, n)$; (ii) each BCE has one and only one pair of diagonally opposite vertices which belong to Ω_1 ; (iii) the space-time E_2 can be filled by $\text{CE}_-(j, n)$ and $\text{CE}_+(j, n)$, $(j, n) \in \Omega_1$; and (iv) $\text{CE}(j, n)$, which is the union of $\text{CE}_-(j, n)$ and $\text{CE}_+(j, n)$, is referred to as a compounded conservation element (CCE).

Note that, among the line segments forming the boundary of $\text{CE}_-(j, n)$, \overline{AB} and \overline{AD} belong to $\text{SE}(j, n)$, while \overline{CB} and \overline{CD} belong to $\text{SE}(j - 1/2, n - 1/2)$. Similarly, among the line segments forming the boundary of $\text{CE}_+(j, n)$, \overline{AF} and \overline{AD} belong to $\text{SE}(j, n)$, while \overline{EF} and \overline{ED} belong to $\text{SE}(j + 1/2, n - 1/2)$. As will be shown, by imposing the two local flux conservation conditions at each $(j, n) \in \Omega_1$, i.e.,

$$\oint_{S(\text{CE}_+(j,n))} \vec{h}^* \cdot d\vec{s} = 0 \quad (j, n) \in \Omega_1 \quad (1.7)$$

and

$$\oint_{S(\text{CE}_-(j,n))} \vec{h}^* \cdot d\vec{s} = 0 \quad (j, n) \in \Omega_1 \quad (1.8)$$

one can obtain two equations for two unknowns u_j^n and $(u_{\bar{x}})_j^n$.

Let

$$\nu \stackrel{\text{def}}{=} a \frac{\Delta t}{\Delta x} \quad \text{and} \quad (u_{\bar{x}})_j^n \stackrel{\text{def}}{=} \frac{\Delta x}{4} (u_x)_j^n \quad (j, n) \in \Omega_1 \quad (1.9)$$

where ν is the Courant number, and $(u_{\bar{x}})_j^n$ is the *normalized* version of $(u_x)_j^n$. Then, with the aid of Eqs. (1.4), (1.6) and (1.9), it can be shown that Eqs. (1.7) and (1.8) are equivalent to

$$(1 - \nu) [u + (1 + \nu)u_{\bar{x}}]_j^n = (1 - \nu) [u - (1 + \nu)u_{\bar{x}}]_{j+1/2}^{n-1/2} \quad (j, n) \in \Omega_1 \quad (1.10)$$

and

$$(1 + \nu) [u - (1 - \nu)u_{\bar{x}}]_j^n = (1 + \nu) [u + (1 - \nu)u_{\bar{x}}]_{j-1/2}^{n-1/2} \quad (j, n) \in \Omega_1 \quad (1.11)$$

respectively. To simplify notation, in the above and hereafter we adopt a convention that can be explained using an expression on the left side of Eq. (1.10) as an example, i.e.,

$$[u + (1 + \nu)u_{\bar{x}}]_j^n = u_j^n + (1 + \nu)(u_{\bar{x}})_j^n$$

By adding Eqs. (1.10) and (1.11) together, one has

$$u_j^n = \frac{1}{2} \left\{ (1 - \nu) [u - (1 + \nu)u_{\bar{x}}]_{j+1/2}^{n-1/2} + (1 + \nu) [u + (1 - \nu)u_{\bar{x}}]_{j-1/2}^{n-1/2} \right\} \quad (j, n) \in \Omega_1 \quad (1.12)$$

Let $1 - \nu^2 \neq 0$, i.e., $1 - \nu \neq 0$ and $1 + \nu \neq 0$. Then Eqs. (1.10) and (1.11) can be divided by $(1 - \nu)$ and $(1 + \nu)$, respectively. By subtracting the resulting equations from each other, one has

$$(u_{\bar{x}})_j^n = \frac{1}{2} \left\{ [u - (1 + \nu)u_{\bar{x}}]_{j+1/2}^{n-1/2} - [u + (1 - \nu)u_{\bar{x}}]_{j-1/2}^{n-1/2} \right\} \quad (j, n) \in \Omega_1 \quad (1.13)$$

Hereafter, by definition the *a* scheme is formed by Eq. (1.12) and (1.13) for any ν . According the above derivation, a solution to the *a* scheme will satisfy Eqs. (1.10) and (1.11) and therefore the two conservation conditions Eqs. (1.7) and (1.8) for any ν . However, because Eqs. (1.7) and (1.8) \Rightarrow (i.e., “imply”) Eq. (1.12) for any ν , but they \Rightarrow Eq. (1.13) only if $\nu^2 \neq 1$, one concludes that a solution to Eqs. (1.7) and (1.8) may not be a solution to the *a* scheme if $\nu^2 = 1$. As such the *a* scheme represents a stronger condition than that of Eq. (1.7) and (1.8).

The *a* scheme is an explicit and neutrally stable (i.e., non-dissipative) solver of Eq. (1.1) in its stability domain $|\nu| < 1$ [63]. Also, according to Eqs. (1.12) and (1.13), it has a space-time staggered stencil, i.e., any $(j, n) \in \Omega_1$ is associated with a stencil formed by the three mesh points (j, n) , $(j - 1/2, n - 1/2)$ and $(j + 1/2, n - 1/2)$.

Eqs. (1.7) and (1.8), i.e., the flux conservation conditions over the two BCEs $\text{CE}_-(j, n)$ and $\text{CE}_+(j, n)$ for all $(j, n) \in \Omega_1$, are enforced by any solution to the *a* scheme. Because (i) the vector \vec{h}^* at any surface element lying on any interface separating two neighboring BCE is evaluated using the information from a

single SE, and (ii) the unit outward normal vector on the surface element pointing outward from one of these two neighboring BCEs is exactly the negative of that pointing outward from another BCE, one concludes that the flux leaving one of these BCEs through the interface is the negative of that leaving another BCE through the same interface. As a result of this flux cancellation, the local flux conservation relations Eqs. (1.7) and (1.8) lead to a global flux conservation relation, i.e., *the total flux of \vec{h}^* leaving the boundary of any space-time region that is the union of any combination of BCEs will also vanish*. In particular, because $\text{CE}(j, n)$ is the union of $\text{CE}_-(j, n)$ and $\text{CE}_+(j, n)$,

$$\oint_{S(\text{CE}(j,n))} \vec{h}^* \cdot d\vec{s} = 0 \quad (j, n) \in \Omega_1 \quad (1.14)$$

must follow from Eqs. (1.7) and (1.8). In fact, *it can be shown that Eq. (1.14) is equivalent to Eq. (1.12)*.

There is a family of the dissipative extensions of the a scheme in which *only the less stringent conservation condition Eq. (1.14) is assumed* [5,26,31,63]. Because Eq. (1.14) is equivalent to Eq. (1.12), for each of these extensions, u_j^n is still evaluated using Eq. (1.12) while $(u_{\bar{x}})_j^n$ is evaluated in terms of the mesh variables at $(j - 1/2, n - 1/2)$ and $(j + 1/2, n - 1/2)$ using an equation different from Eq. (1.13). In fact, (i) the a - ϵ scheme is formed by Eq. (1.12) and

$$(u_{\bar{x}})_j^n = \frac{1}{2} \left\{ [(1 - \epsilon)u + (2\epsilon - 1 - \nu)u_{\bar{x}}]_{j+1/2}^{n-1/2} - [(1 - \epsilon)u + (1 - \nu - 2\epsilon)u_{\bar{x}}]_{j-1/2}^{n-1/2} \right\} \quad (j, n) \in \Omega_1 \quad (1.15)$$

where ϵ is a real parameter, and (ii) the c - τ scheme is formed by Eq. (1.12) and

$$(u_{\bar{x}})_j^n = \frac{1}{2(1 + \tau)} \left\{ [u - (1 + 2\nu - \tau)u_{\bar{x}}]_{j+1/2}^{n-1/2} - [u + (1 - 2\nu - \tau)u_{\bar{x}}]_{j-1/2}^{n-1/2} \right\} \quad (j, n) \in \Omega_1 \quad (1.16)$$

where τ is a real parameter $\neq -1$.

Note that:

- (a) By comparing Eqs. (1.13) and (1.15), it is seen that the a scheme is the special case of the a - ϵ scheme when $\epsilon = 0$.
- (b) By using Jordan canonical form theorem [71], it can be shown that the a - ϵ scheme is von Neumann stable \Leftrightarrow (i.e., “if and only if”) either

$$0 \leq \epsilon \leq 1 \quad \text{and} \quad |\nu| < 1 \quad (1.17)$$

or

$$\epsilon = |\nu| = 1 \quad (1.18)$$

Also one can show that the a - ϵ scheme becomes more dissipative as the value of ϵ increases from 0 to 1 [5].

- (c) By using Jordan canonical form theorem [71], it is shown rigorously in [46] that the c - τ scheme is von Neumann stable \Leftrightarrow

$$\nu^2 \leq 1, \quad \tau \geq \tau_o(\nu^2), \quad \text{and} \quad (\nu^2, \tau) \neq (1, 1) \quad (1.19)$$

where

$$\tau_o(s) \stackrel{\text{def}}{=} \begin{cases} 0 & \text{if } s = 0 \\ \frac{4 - s - 2\sqrt{2(2 - s - s^2)}}{s} & \text{if } 0 < s \leq \frac{3}{11} \\ \frac{s - 1 + \sqrt{1 - 2s + 5s^2}}{2s} & \text{if } \frac{3}{11} \leq s \leq 1 \end{cases} \quad (1.20)$$

It can be shown that: (i) $\tau_o(s)$ is continuous at $s = 0$, i.e.,

$$\lim_{s \rightarrow 0^+} \tau_o(s) = \tau_o(0) = 0 \quad (1.21)$$

(ii) $\tau_o(s)$ is consistently defined at $s = 3/11$, i.e., both the second and third expressions on the right side of Eq. (1.20) implies that $\tau_o(3/11) = 1/3$; (iii) $\tau_o(s)$ is continuously differentiable at $s = 3/11$, i.e.,

$$\lim_{s \rightarrow \frac{3}{11}^-} \tau'_o(s) = \lim_{s \rightarrow \frac{3}{11}^+} \tau'_o(s) = 121/90 \quad (1.22)$$

where $\tau'_o(s) \stackrel{\text{def}}{=} d\tau_o(s)/ds$; (iv) $\tau_o(s)$ is strictly monotonically increasing in the interval $0 < s < 1$; (v) $\tau_o(1) = 1$; and (vi)

$$s < \tau_o(s) < \sqrt{s}, \quad 0 < s < 1 \quad (1.23)$$

Moreover, (i) the stability conditions Eq. (1.19) agree completely with those generated through numerical experiments [31] (Note: the reader is warned that the condition $\tau \geq \tau_o(\nu^2)$ that appears in Eq. (1.19) here is expressed as $\tau \geq \tau_o(|\nu|)$ in Eq. (3.12) of [31], i.e., the function τ_o defined here is *different* from the function τ_o introduced in [31]), and (ii) for any given fixed value of $|\nu| < 1$, the c - τ scheme tends to become more dissipative as the value of τ increases from its minimum stability bound $\tau_o(\nu^2)$.

The a scheme and its extensions were defined over Ω_1 , the set of space-time staggered mesh points marked by dots in Fig. 2(a). Obviously, the a scheme can also be defined over Ω_2 , the set of all space-time staggered mesh points (j, n) in E_2 where $n = 0, \pm 1/2, \pm 1, \pm 3/2, \pm 2, \dots$, and, for each n , $j = n, n \pm 1, n \pm 2, n \pm 3, \dots$. By definition, each $(j, n) \in \Omega_2$ is associated with a whole-integer value of $(j + n)$, and represented by a mesh point not marked by dots in Fig. 2(a). Because one can carry out the time marching (using the a scheme or any one of its 1D extensions) exclusively over either Ω_1 or Ω_2 , there is no need to carry out a marching over both Ω_1 and Ω_2 . Note that this conclusion generally remains valid even if an 1D nonuniform spatial mesh is used [31]. The exception may occur for a marching scheme where the time-step size varies from one spatial region to another such as the local time stepping procedure described in [42].

Note that the two disjoint sets Ω_1 and Ω_2 have the property that, if a space-time mesh point (j, n) belongs to Ω_1 (Ω_2), then its four immediate space-time neighbors $(j \pm 1/2, n)$ and $(j, n \pm 1/2)$ must belong to Ω_2 (Ω_1). As a result, for a scheme with a space-time staggered stencil such as the a scheme or the classical leapfrog scheme, this implies that a time marching carried out over Ω_1 is completely decoupled from that carried out over Ω_2 . As such one only needs to carry out time marching over one of these two sets. For this reason, the problem of “solution decoupling” (which is famously associated with the leapfrog scheme) usually can be avoided in the 1D case.

However, as will be shown shortly, for a space-time mesh built from a multidimensional *unstructured* spatial mesh, one generally cannot define two disjoint sets of space-time mesh points which possess the same property of Ω_1 and Ω_2 discussed above. As such, the problem of solution decoupling may become a real nuisance in multidimensional CESE simulations involving unstructured spatial meshes.

As was shown earlier that, for an 1D CESE scheme, (i) each mesh point is assigned with two BCEs; and (ii) for each dependent physical variable u , each mesh point (j, n) is assigned with two independent mesh variables u_j^n and $(u_x)_j^n$. Similarly [12,13], for a 2D (3D) CESE scheme, (i) each space-time solution point (to be defined shortly) is assigned with three (four) BCEs and one CCE, with the CCE being the union of the three (four) BCEs; and (ii) for each dependent physical variable, each space-time solution point is assigned with three (four) independent mesh variables—note that there are two (three) independent spatial derivatives in a problem with two (three) spatial dimension. *Because a triangle and a tetrahedron have three and four sides, respectively, triangles and tetrahedra, respectively, become the simplest and most natural building blocks of the spatial meshes for 2D and 3D CESE schemes* [10–13,16]. As such, in the following discussion about solution decoupling in a CESE simulation involving an unstructured 2D spatial domain, we consider an unstructured domain built from triangles.

Consider a spatial domain formed by triangles of arbitrary shapes (see Fig. 3). Here (i) any two neighboring triangles share a common side, and (ii) the vertices and centroids of triangles are marked by dots and circles, respectively. As shown in Fig. 3, the triangle $\triangle FBD$ has three neighboring triangles. Let (i) point G be the centroid of $\triangle FBD$, and (ii) points A , C and E , respectively, be the centroids of the three neighbors of $\triangle FBD$. Then points A , B , C , D , E , and F form a hexagon. The centroid of the hexagon

is denoted by G' and marked by a cross. Hereafter point G' is referred to as the spatial solution point of $\triangle FBD$. In a similar manner, we define spatial solution points A' , C' , E' ,... of other triangles.

A space-time solution point is a mesh point which resides at a time level $n = 0, 1/2, 1, 3/2, 2, \dots$ ($t = t^n = n\Delta t$ at the n th time level) and has a spatial solution point being its spatial projection. Given any spatial solution point G' and any time level n , let (G', n) denote the space-time solution point which resides at the n th time level and has point G' being its spatial projection. As explained in [13], the three BCEs associated with (G', n) are constructed such that their spatial projections are the quadrilaterals $GFAB$, $GBCD$, and $GDEF$, respectively. Also, for a reason explained in [13], independent mesh variables are stored at space-time solution points.

As shown in [13], in a 2D CESE scheme using a triangular spatial mesh, the mesh variables at (G', n) are evaluated in terms of those at $(A', n - 1/2)$, $(C', n - 1/2)$ and $(E', n - 1/2)$, i.e., the scheme has a space-time staggered stencil formed by one point at the n th time level and three points at the $(n - 1/2)$ th time level. Also it was shown in [13] that, *given an unstructured triangular spatial mesh, the time marching cannot be carried out independently over two disjoint sets of space-time solution points unless the triangles forming the spatial mesh can be divided into two disjoint sets Ψ_1 and Ψ_2 such that two triangles sharing a common side always belong to two different sets.* As will be shown, because point F is the common vertex of an odd number (5) of triangles, the triangles depicted in Fig. 3 cannot be divided into Ψ_1 and Ψ_2 .

To prove the last proposition by contradiction, let $\triangle FBD \in \Psi_1$. Then because $\triangle FHB$ and $\triangle FBD$ share a common side, by definition, $\triangle FHB \in \Psi_2$. Similarly, because (i) $\triangle FNH$ and $\triangle FHB$ share a common side, (ii) $\triangle FMN$ and $\triangle FNH$ share a common side, and (iii) $\triangle FDM$ and $\triangle FMN$ share a common side, one concludes that $\triangle FNH \in \Psi_1$, $\triangle FMN \in \Psi_2$, and $\triangle FDM \in \Psi_1$. As such, we have arrived at the contradiction that both $\triangle FBD$ and $\triangle FDM$ belong to Ψ_1 in spite of the fact that they share a common side. Because we will reach a similar contradiction by assuming $\triangle FBD \in \Psi_2$, the proposition has been proved.

The triangles depicted in Fig. 3 cannot be divided into two disjoint sets Ψ_1 and Ψ_2 . As such, according to another proposition stated earlier, the CESE time marching cannot be carried out independently over two disjoint sets of space-time solution points constructed from the triangular spatial mesh depicted in Fig. 3. Moreover, because the incidence that an odd number of triangles sharing a common vertex occurs regularly in an unstructured triangular mesh, the CESE time marching generally cannot be carried out independently over two disjoint sets of space-time solution points if they are constructed from an unstructured triangular spatial mesh.

Similarly, for a 3D CESE scheme using an unstructured spatial mesh built from tetrahedra, it can be shown that generally the time marching cannot be carried out independently over two disjoint sets of space-time staggered solution points.

According to the above discussions, a CESE multidimensional time marching using an unstructured triangular or tetrahedral spatial mesh generally will involve all space-time solution points. This coupled with the fact that a CESE scheme has a space-time staggered stencil implies that solution decoupling may become a real nuisance. To deal with this problem once and for all, recently new CESE schemes have been developed such that possibility of solution decoupling can be removed completely. The description of these new schemes is one of the topics covered in the current paper. As will be shown, (i) these new schemes are constructed without compromising the basic CESE ideas, and (ii) their effectiveness has been verified by real-world applications. [62, 64–67].

To describe another topic of the current paper, note that the spatial solution point G' depicted in Fig. 3 is the centroid of the hexagon $ABCDEF$ where points A , C and E , respectively, are rather arbitrarily designated as the centroids of the three neighbors of $\triangle FBD$. *In fact, to insure that CEs will not overlap in space and thus no loss of local and global flux conservation will occur, it only requires that points such as G , A , C and E lie in the interiors of $\triangle FBD$, $\triangle FHB$, $\triangle BLD$, and $\triangle FDM$, respectively.*

For the rather benign triangular domain depicted in Fig. 3, the hexagon $ABCDEF$ happens to be convex, i.e., a line segment joining any two points in this hexagon always lies entirely in it. Because the centroid of a convex polygon always lies within its interior, the centroid (i.e., point G') of the hexagon $ABCDEF$ lies within its interior. However, this may not be true for a more pathological triangular domain

formed from triangles with very large aspect ratios and sharply different orientations. As an example, consider Fig. 4 where $\triangle FBD$ is again surrounded by three neighboring triangles $\triangle FHB$, $\triangle BLD$ and $\triangle FDM$. However, in Fig. 4, the aspect ratio of each of the four triangles depicted is much larger than that of its counterpart depicted in Fig. 3. Moreover, in Fig. 4, the orientations of the sides \overline{BD} and \overline{FD} of $\triangle FBD$ are sharply different from those of the sides \overline{BH} and \overline{FH} of $\triangle FHB$, respectively. Let points G , A , C and E depicted in Fig. 4 again be the centroids of $\triangle FBD$, $\triangle FHB$, $\triangle BLD$, and $\triangle FDM$, respectively. Then the resulting hexagon $ABCDEF$ may become highly concave and thus its centroid G' (not shown in Fig. 4) may no longer lie in its interior.

Similarly, a CESE tetrahedral mesh is built from tetrahedra where any two neighboring tetrahedra share a common triangular face. Given any two neighboring tetrahedra, in the original CESE tetrahedral-mesh construction, the 5-vertex polyhedron with its vertices being (i) the centroids of these two neighbors and (ii) the three vertices of the triangular face shared by them, becomes the spatial projection of a BCE. Because each tetrahedron is associated with four neighbors, it is associated with four 5-vertex polyhedra and their union—a 8-vertex polyhedron. The 8-vertex polyhedron and its centroid, respectively, are the spatial projections of a CCE and a spatial solution point. For some pathological case where the 8-vertex polyhedron becomes highly concave, its centroid (i.e., the spatial solution point associated with this polyhedron) may lie outside of its interior.

In a real-world CFD simulation near a solid wall, one often encounters a case where a boundary with high curvature or sharp corner is surrounded by triangular/tetrahedral meshes of extremely high aspect ratio (up to 10^6). For such an extreme case, a spatial solution point may lie far outside of the associated hexagon/8-vertex polyhedron. It could even be embedded beyond a solid-wall boundary and causes serious numerical difficulties. To overcome this problem, a new way of building spatial meshes from triangles and tetrahedra has been developed. Specifically, the centroids of *triangles* depicted in Fig. 3 have been replaced by the corresponding *in-centers* or other specially-defined interior points in the new construction. However, the solution point is still the centroid of the new hexagon formed by vertices and in-centers (or other specially-defined interior points). Similarly, centroids of tetrahedra also are replaced by corresponding in-centers or other specially-defined interior points in the new construction. According to the numerical results obtained [62,64,65], the new construction has the following advantages: (i) it can properly model curved boundaries—without it, computed surface gradient such as heat flux will be much less accurate (and noisier in many cases); (ii) it can reduce aspect ratios of triangular or tetrahedral cells used in gradient calculations in a highly stretched mesh and, as a result, can improve the overall accuracy for triangular and tetrahedral meshes; (iii) for vortex-shedding problems, better resolution is observed by using the in-center formulation. In this paper we will describe this new development and also provide the theoretical justification for the new construction.

As mentioned earlier, mesh values of the physical dependent variables and their spatial derivatives are treated as independent mesh variables in a CESE scheme. As it turns out, for a case where a triangular or tetrahedral mesh is used, numerical evaluation of the spatial derivatives using the established CESE approach tends to become less accurate as the mesh cell aspect ratio becomes larger. In the latest development, the root cause behind this tendency was clearly identified and several remedies to overcome it were found through a rigorous mathematical analysis. However, because of the length of the current paper and the complexity of the mathematics involved, this latest work will be presented in another paper.

Because it is rather simple and straightforward, in the following, first we will describe the new way of building spatial meshes from triangles and tetrahedra. The new flux-conserving solution-coupling procedures will be presented in Sec. 3.

2. New construction of triangular and tetrahedral meshes

2.1. Triangular meshes

Again consider the triangle $\triangle FBD$ and the hexagon $ABCDEF$ depicted in Fig. 4. As noted earlier, (i) because it is the centroid of the hexagon $ABCDEF$, the spatial solution point G' (not shown in Fig. 4) always lies in the interior of the hexagon if it is convex but may lie outside of it if it is concave; and (ii) serious numerical difficulties may arise if point G' lies outside of the hexagon $ABCDEF$. As such, to avoid

numerical difficulties, it is essential to ensure that $ABCDEF$ is a convex hexagon.

Because any triangle such as $\triangle FBD$ is always convex, the hexagon $ABCDEF$ will also be convex if its boundary more or less coincides with that of $\triangle FBD$. In other words, the hexagon is convex if points A , C , and E are located close enough to the sides \overline{BF} , \overline{BD} and \overline{FD} , respectively. Unfortunately, because (i) A is the centroid of $\triangle FHB$, and (ii)

$$|\overline{BF}| \ll |\overline{BH}| \quad \text{and} \quad |\overline{BF}| \ll |\overline{FH}| \quad (2.1)$$

(hereafter, as an example, the length of \overline{BF} is denoted by $|\overline{BF}|$), point A generally is far away from the side \overline{BF} . As such the hexagon $ABCDEF$ may become concave. For this reason and the previously stated requirement that point A , C , and E must lie in the interiors of $\triangle FHB$, $\triangle BLD$, and $\triangle FDM$, respectively, in the following, we will describe a new approach in which the locations of A , C , and E are chosen so that: (i) each of them again is an interior point of the associated triangle, and (ii) a point such as A will remain close to the side \overline{BF} even for the pathological case Eq. (2.1).

Consider Fig. 5. Here (i) points P_1 , P_2 , P_3 are the vertices of the triangle $\triangle P_1P_2P_3$ which lies on the x - y plane and has its area

$$A(\triangle P_1P_2P_3) > 0 \quad (2.2)$$

(ii) P_0 is a point on the x - y plane to be defined shortly; (iii) for each $k = 0, 1, 2, 3$, x_k and y_k are the x - and y - coordinates of point P_k , respectively; (iv) point Q_1 is the point on $\overline{P_2P_3}$ (or its extension) which meets the condition

$$\overline{P_0Q_1} \perp \overline{P_2P_3} \quad (2.3)$$

i.e., Q_1 is the perpendicular projection of P_0 on the straight line which contains $\overline{P_2P_3}$; (v) point Q_2 is the point on $\overline{P_3P_1}$ (or its extension) which meets the condition

$$\overline{P_0Q_2} \perp \overline{P_3P_1} \quad (2.4)$$

i.e., Q_2 is the perpendicular projection of P_0 on the straight line which contains $\overline{P_3P_1}$; (vi) point Q_3 is the point on $\overline{P_1P_2}$ (or its extension) which meets the condition

$$\overline{P_0Q_3} \perp \overline{P_1P_2} \quad (2.5)$$

i.e., Q_3 is the perpendicular projection of P_0 on the straight line which contains $\overline{P_1P_2}$; (vii) α_1 , α_2 , and α_3 are the internal angles of $\triangle P_1P_2P_3$ facing the sides $\overline{P_2P_3}$, $\overline{P_3P_1}$, and $\overline{P_1P_2}$, respectively; (viii)

$$\ell_1 \stackrel{\text{def}}{=} |\overline{P_2P_3}|, \quad \ell_2 \stackrel{\text{def}}{=} |\overline{P_3P_1}| \quad \text{and} \quad \ell_3 \stackrel{\text{def}}{=} |\overline{P_1P_2}| \quad (2.6)$$

(ix)

$$h_k \stackrel{\text{def}}{=} |\overline{P_0Q_k}| \quad k = 1, 2, 3 \quad (2.7)$$

and (x) the x - y - z coordinate system depicted in Fig. 5 is a right-handed system, i.e.,

$$\vec{e}_x \times \vec{e}_y = \vec{e}_z, \quad \vec{e}_y \times \vec{e}_z = \vec{e}_x \quad \text{and} \quad \vec{e}_z \times \vec{e}_x = \vec{e}_y \quad (2.8)$$

where \vec{e}_x , \vec{e}_y , and \vec{e}_z are the unit vectors in the x -, y -, and z - directions, respectively.

Note that, according to Eq. (2.6) and Fig. 5, for each $k = 1, 2, 3$, ℓ_k denotes the length of the side of $\triangle P_1P_2P_3$ facing the vertex P_k . Also from the definition of points Q_1 , Q_2 , and Q_3 , and that of h_k , $k = 1, 2, 3$, one concludes that h_1 , h_2 , and h_3 , respectively, are the (shortest) distances from P_0 to the straight lines that contain the sides $\overline{P_2P_3}$, $\overline{P_3P_1}$, and $\overline{P_1P_2}$, respectively.

For each $k = 0, 1, 2, 3$, let \vec{P}_k be the position vector of point P_k , i.e.,

$$\vec{P}_k \stackrel{\text{def}}{=} x_k \vec{e}_x + y_k \vec{e}_y \quad k = 0, 1, 2, 3 \quad (2.9)$$

Also let \vec{P}_0 be an weighted average of \vec{P}_k , $k = 1, 2, 3$, i.e.,

$$\vec{P}_0 = w_1 \vec{P}_1 + w_2 \vec{P}_2 + w_3 \vec{P}_3 \quad (2.10)$$

where w_1, w_2 , and w_3 are real weight factors with

$$w_1 + w_2 + w_3 = 1 \quad (2.11)$$

Moreover, given a pair of integers k_1 and k_2 with $k_1 \neq k_2$ and $k_1, k_2 = 0, 1, 2, 3$, let $\overrightarrow{P_{k_1}P_{k_2}}$ be the displacement vector joining points P_{k_1} and P_{k_2} and pointing in the direction from P_{k_1} to P_{k_2} , i.e.,

$$\overrightarrow{P_{k_1}P_{k_2}} \stackrel{\text{def}}{=} \vec{P}_{k_2} - \vec{P}_{k_1}, \quad k_1 \neq k_2 \quad \text{and} \quad k_1, k_2 = 0, 1, 2, 3 \quad (2.12)$$

Then, by using Eq. (2.12) and other well-known properties of the vector product such as

$$\vec{A} \times \vec{A} = 0 \quad \text{and} \quad \vec{A} \times \vec{B} = -\vec{B} \times \vec{A} \quad (2.13)$$

for any vectors \vec{A} and \vec{B} , one can show that

$$\overrightarrow{P_1P_2} \times \overrightarrow{P_1P_3} = (\vec{P}_2 - \vec{P}_1) \times (\vec{P}_3 - \vec{P}_1) = \vec{P}_1 \times \vec{P}_2 + \vec{P}_2 \times \vec{P}_3 + \vec{P}_3 \times \vec{P}_1 \quad (2.14)$$

Similarly, with the aid of Eqs. (2.10)–(2.14), one can show that

$$\overrightarrow{P_0P_2} \times \overrightarrow{P_0P_3} = w_1 (\vec{P}_1 \times \vec{P}_2 + \vec{P}_2 \times \vec{P}_3 + \vec{P}_3 \times \vec{P}_1) = w_1 (\overrightarrow{P_1P_2} \times \overrightarrow{P_1P_3}) \quad (2.15)$$

$$\overrightarrow{P_0P_3} \times \overrightarrow{P_0P_1} = w_2 (\vec{P}_1 \times \vec{P}_2 + \vec{P}_2 \times \vec{P}_3 + \vec{P}_3 \times \vec{P}_1) = w_2 (\overrightarrow{P_1P_2} \times \overrightarrow{P_1P_3}) \quad (2.16)$$

$$\overrightarrow{P_0P_1} \times \overrightarrow{P_0P_2} = w_3 (\vec{P}_1 \times \vec{P}_2 + \vec{P}_2 \times \vec{P}_3 + \vec{P}_3 \times \vec{P}_1) = w_3 (\overrightarrow{P_1P_2} \times \overrightarrow{P_1P_3}) \quad (2.17)$$

Next, by using (i) a well-known property of the vector product, (ii) the fact that $A(\triangle P_1P_2P_3)$ denotes the area of $\triangle P_1P_2P_3$, and (iii) Fig. 5, one has

$$A(\triangle P_1P_2P_3) = (|\overrightarrow{P_1P_2}| |\overrightarrow{P_1P_3}| \sin \alpha_1) / 2 = |\overrightarrow{P_1P_2} \times \overrightarrow{P_1P_3}| / 2 \quad (2.18)$$

Similarly, with the aid of Eqs. (2.15)–(2.18), one can show that

$$A(\triangle P_0P_2P_3) = |\overrightarrow{P_0P_2} \times \overrightarrow{P_0P_3}| / 2 = |w_1| \times A(\triangle P_1P_2P_3) \quad (2.19)$$

$$A(\triangle P_0P_3P_1) = |\overrightarrow{P_0P_3} \times \overrightarrow{P_0P_1}| / 2 = |w_2| \times A(\triangle P_1P_2P_3) \quad (2.20)$$

and

$$A(\triangle P_0P_1P_2) = |\overrightarrow{P_0P_1} \times \overrightarrow{P_0P_2}| / 2 = |w_3| \times A(\triangle P_1P_2P_3) \quad (2.21)$$

where $A(\triangle P_0P_2P_3)$, $A(\triangle P_0P_3P_1)$, and $A(\triangle P_0P_1P_2)$ denote the areas of $\triangle P_0P_2P_3$, $\triangle P_0P_3P_1$, and $\triangle P_0P_1P_2$, respectively. In turn, Eqs. (2.19)–(2.21) \Rightarrow

$$A(\triangle P_0P_2P_3) + A(\triangle P_0P_3P_1) + A(\triangle P_0P_1P_2) = (|w_1| + |w_2| + |w_3|) \times A(\triangle P_1P_2P_3) \quad (2.22)$$

Because a triangle such as $\triangle P_1P_2P_3$ is intrinsically convex, according to a theorem on convex sets, *point P_0 defined by Eqs. (2.10) and (2.11) lies on the boundary or in the interior of $\triangle P_1P_2P_3$* \Leftrightarrow

$$0 \leq w_k \leq 1 \quad k = 1, 2, 3 \quad (2.23)$$

Moreover, because Eq. (2.2) implies that the interior of $\triangle P_1P_2P_3$ is not empty, P_0 lies in the interior of $\triangle P_1P_2P_3 \Leftrightarrow$

$$0 < w_k < 1 \quad k = 1, 2, 3 \quad (2.24)$$

For the case where P_0 lies on the boundary or in the interior of $\triangle P_1P_2P_3$, Eqs. (2.11), (2.22), and (2.23) now \Rightarrow the following obvious result:

$$A(\triangle P_0P_2P_3) + A(\triangle P_0P_3P_1) + A(\triangle P_0P_1P_2) = A(\triangle P_1P_2P_3) \quad (2.25)$$

On the other hand, for the case where P_0 lies outside of $\triangle P_1P_2P_3$, Eq. (2.23) is no longer true, i.e., some of the weight factors must be negative. Because Eq. (2.11) requires that some of the weight factors must be positive, we arrive at the conclusion that

$$|w_1| + |w_2| + |w_3| > |w_1 + w_2 + w_3| = 1 \quad (2.26)$$

if P_0 lies outside of $\triangle P_1P_2P_3$. In turn, Eqs. (2.22) and (2.26) \Rightarrow

$$A(\triangle P_0P_2P_3) + A(\triangle P_0P_3P_1) + A(\triangle P_0P_1P_2) > A(\triangle P_1P_2P_3) \quad (2.27)$$

if P_0 lies outside of $\triangle P_1P_2P_3$.

Note that, for any real parameter ζ , Eqs. (2.2) and (2.6) \Rightarrow

$$\ell_k > 0 \quad \text{and} \quad (\ell_k)^\zeta > 0 \quad k = 1, 2, 3; \quad -\infty < \zeta < +\infty \quad (2.28)$$

As such the weight factors

$$w_k(\zeta) \stackrel{\text{def}}{=} \frac{(\ell_k)^\zeta}{(\ell_1)^\zeta + (\ell_2)^\zeta + (\ell_3)^\zeta} \quad k = 1, 2, 3; \quad -\infty < \zeta < +\infty \quad (2.29)$$

are well defined and satisfy the conditions

$$0 < w_k(\zeta) < 1 \quad k = 1, 2, 3, \quad -\infty < \zeta < +\infty \quad (2.30)$$

and

$$w_1(\zeta) + w_2(\zeta) + w_3(\zeta) = 1 \quad -\infty < \zeta < +\infty \quad (2.31)$$

In this subsection hereafter we consider only the special case where

$$w_k = w_k(\zeta) \quad k = 1, 2, 3; \quad -\infty < \zeta < +\infty \quad (2.32)$$

For this special case, Eqs. (2.30)–(2.32) imply that both Eqs. (2.11) and (2.24) are satisfied for any real number ζ . Thus, for the case Eq. (2.32), (i) *point P_0 defined by Eq. (2.10) must always lie in the interior of $\triangle P_1P_2P_3$* , and (ii) Eqs. (2.19)–(2.22) reduce to

$$A(\triangle P_0P_2P_3) = w_1 \times A(\triangle P_1P_2P_3) \quad (2.33)$$

$$A(\triangle P_0P_3P_1) = w_2 \times A(\triangle P_1P_2P_3) \quad (2.34)$$

$$A(\triangle P_0P_1P_2) = w_3 \times A(\triangle P_1P_2P_3) \quad (2.35)$$

and Eq. (2.25), respectively. Moreover, for the special case $\zeta = 0$, we have

$$w_1 = w_2 = w_3 = 1/3 \quad \text{and} \quad \vec{P}_0 = \left(\vec{P}_1 + \vec{P}_2 + \vec{P}_3 \right) / 3 \quad (\zeta = 0) \quad (2.36)$$

Because the position vector of the centroid of a triangle is the simple average of those of its three vertices, Eq. (2.36) \Rightarrow point P_0 is the centroid of $\triangle P_1P_2P_3$ if $\zeta = 0$.

Note that, for a polygon other than a triangle (which is the simplest polygon), generally it is not true that the position vector of its centroid is the simple average of those of its vertices. As an example, *the position vector of the centroid of a quadrilateral may not be the simple average of those of its four vertices unless the quadrilateral is a parallelogram.*

Next, with the aid of Eqs. (2.6) and (2.7), and Fig. 5, one can see that

$$A(\triangle P_0P_2P_3) = \frac{h_1\ell_1}{2}, \quad A(\triangle P_0P_3P_1) = \frac{h_2\ell_2}{2} \quad \text{and} \quad A(\triangle P_0P_1P_2) = \frac{h_3\ell_3}{2} \quad (2.37)$$

In turn, by substituting Eq. (2.37) into Eqs. (2.33)–(2.35) and using Eqs. (2.29) and (2.32), one has

$$\frac{h_k\ell_k}{2} = w_k A(\triangle P_1P_2P_3) = \frac{(\ell_k)^\zeta \times A(\triangle P_1P_2P_3)}{(\ell_1)^\zeta + (\ell_2)^\zeta + (\ell_3)^\zeta} \quad k = 1, 2, 3; \quad -\infty < \zeta < +\infty \quad (2.38)$$

and thus

$$\frac{h_1}{(\ell_1)^{\zeta-1}} = \frac{h_2}{(\ell_2)^{\zeta-1}} = \frac{h_3}{(\ell_3)^{\zeta-1}} = \frac{2 \times A(\triangle P_1P_2P_3)}{(\ell_1)^\zeta + (\ell_2)^\zeta + (\ell_3)^\zeta} \quad -\infty < \zeta < +\infty \quad (2.39)$$

Because (i) h_1 , h_2 and h_3 are the distances from point P_0 to the sides $\overline{P_2P_3}$, $\overline{P_3P_1}$, and $\overline{P_1P_2}$, respectively, and (ii) ℓ_1 , ℓ_2 , and ℓ_3 are the lengths of $\overline{P_2P_3}$, $\overline{P_3P_1}$, and $\overline{P_1P_2}$, respectively, Eq. (2.39) states that, for a given $\triangle P_1P_2P_3$ and a given ζ , the distance from point P_0 to any side of $\triangle P_1P_2P_3$ is proportional to the $(\zeta - 1)$ th power of the length of this side.

In fact, for the case $\zeta = 0$ (i.e., when P_0 is the centroid of $\triangle P_1P_2P_3$), Eq. (2.39) reduces to

$$h_k = \left[\frac{2 \times A(\triangle P_1P_2P_3)}{3} \right] \frac{1}{\ell_k} \quad k = 1, 2, 3 \quad \text{if} \quad \zeta = 0 \quad (2.40)$$

i.e., the distance between the centroid P_0 and a side of $\triangle P_1P_2P_3$ is inversely proportional to the side length. Thus the centroid is farthest away from the shortest side and closest to the longest side—a result consistent with what we observe from the triangle $\triangle FHB$ depicted in Fig. 4.

On the other hand, for the case $\zeta = 1$, Eq. (2.39) reduces to

$$h_1 = h_2 = h_3 = \frac{2 \times A(\triangle P_1P_2P_3)}{\ell_1 + \ell_2 + \ell_3} \quad \text{if} \quad \zeta = 1 \quad (2.41)$$

i.e., point P_0 has the same distance to the three sides of $\triangle P_1P_2P_3$ if $\zeta = 1$. By definition, this implies that P_0 is the *in-center* of $\triangle P_1P_2P_3$ for the case $\zeta = 1$.

In general one can infer from Eq. (2.39) that:

- (a) For the case $\zeta > 1$, point P_0 is farthest away from the longest side of $\triangle P_1P_2P_3$ and closest to its shortest side. The trend becomes stronger as the value of ζ increases from 1.
- (b) For the case $\zeta < 1$, point P_0 is farthest away from the shortest side of $\triangle P_1P_2P_3$ and closest to its longest side. The trend becomes stronger as the value of ζ decreases from 1.

Let the interior point P_0 of any triangle $\triangle P_1P_2P_3$ defined by Eqs. (2.10) and (2.32) be referred to as *the interior point of this triangle associated with the parameter ζ* . Then, from the above observations and the discussions given in Sec. 1, it becomes clear that a *spatial solution point* such as the point G' depicted in Fig. 3 will be much less likely to lie outside of the associated hexagon $ABCDEF$ and causes numerical difficulties if each of the centroidal mesh points A , C , G and E depicted in Figs. 3 and 4 is replaced by a an interior point associated with a parameter $\zeta \geq 1$. In fact, it has been shown through numerical experiments that the numerical difficulties associated with spatial solution points being embedded beyond a solid-wall boundary can be overcome by replacing centroids of triangles with in-centers (i.e., interior points associated with $\zeta = 1$) in the construction of a spatial triangular mesh.

2.2. Tetrahedral meshes

Consider a 3D spatial domain formed by tetrahedra with the understanding that any two neighboring tetrahedra share a common triangular face. As an example, consider the tetrahedron $P_1P_2P_3P_4$ depicted in Fig. 6(a) where P_1, P_2, P_3 and P_4 are the vertices of the tetrahedron. The tetrahedron has four triangular faces, i.e., $\triangle P_1P_2P_3, \triangle P_2P_3P_4, \triangle P_3P_4P_1$, and $\triangle P_4P_1P_2$. As shown in Fig. 6(b), the tetrahedron $P_1P_2P_3P_4$ shares these faces with four neighboring tetrahedra, i.e., $P_1P_2P_3D, P_2P_3P_4A, P_3P_4P_1B$, and $P_4P_1P_2C$, respectively. Note that, to simplify notation, the same symbols used in Sec. 2.1 may also be used in this subsection albeit that those used here generally denote objects in the 3D x - y - z space.

Because a tetrahedron is intrinsically convex in a 3D x - y - z space, its centroid must lie in its interior if its volume > 0 . Hereafter, only tetrahedra of volume > 0 will be considered. In particular, we assume that

$$V(P_1P_2P_3P_4) \stackrel{\text{def}}{=} \text{the volume of the tetrahedron } P_1P_2P_3P_4 > 0 \quad (2.42)$$

Let the points P_0, A_0, B_0, C_0 , and D_0 depicted in Fig. 6(b) be the centroids of the tetrahedra, $P_1P_2P_3P_4, P_2P_3P_4A, P_3P_4P_1B, P_4P_1P_2C$, and $P_1P_2P_3D$, respectively. Then each of these five centroids lies in the interior of the associated tetrahedron. *As such the four polyhedra $P_0P_2P_3P_4A_0, P_0P_3P_4P_1B_0, P_0P_4P_1P_2C_0$, and $P_0P_1P_2P_3D_0$ (each of them has five vertices, six triangular faces, and nine edges) do not overlap.* In the original CESE 3D tetrahedral mesh construction, (i) each of these 5-vertex polyhedra is the spatial projection of a BCE, (ii) the union of the above four 5-vertex polyhedra is a polyhedron with 8 vertices, 12 triangular faces, and 18 edges, and also is the spatial projection of a CCE, and (iii) the centroid of the 8-vertex polyhedron referred to above is a spatial solution point, i.e., the spatial projection of a space-time solution point.

As in the 2D case, for some pathological case where an 8-vertex polyhedron become highly concave, its centroid (i.e., the associated spatial solution point) may lie outside of the polyhedron and causes numerical difficulties. In the following, we explain how these difficulties can be overcome by a new construction of 3D tetrahedral meshes.

Consider Fig. 6(a) again. Here (i) P_0 is a point in the x - y - z space to be defined shortly and not necessary the centroid of the tetrahedron $P_1P_2P_3P_4$; (ii) for each $k = 0, 1, 2, 3, 4$, x_k, y_k , and z_k are the x -, y - and z -coordinates of point P_k , respectively; (iii) point Q_1 (not shown in Fig. 6(a)) is the point that lies on the plane containing the face $\triangle P_2P_3P_4$, and also meets the condition

$$\overline{P_0Q_1} \perp \triangle P_2P_3P_4 \quad (2.43)$$

i.e., Q_1 is the perpendicular projection of P_0 on the plane containing $\triangle P_2P_3P_4$; (iv) point Q_2 (not shown) is the point that lies on the plane containing the face $\triangle P_3P_4P_1$, and also meets the condition

$$\overline{P_0Q_2} \perp \triangle P_3P_4P_1 \quad (2.44)$$

i.e., Q_2 is the perpendicular projection of P_0 on the plane containing $\triangle P_3P_4P_1$; (v) point Q_3 (not shown) is the point that lies on the plane containing the face $\triangle P_4P_1P_2$, and also meets the condition

$$\overline{P_0Q_3} \perp \triangle P_4P_1P_2 \quad (2.45)$$

i.e., Q_3 is the perpendicular projection of P_0 on the plane containing $\triangle P_4P_1P_2$; (vi) point Q_4 (not shown) is the point that lies on the plane containing the face $\triangle P_1P_2P_3$, and also meets the condition

$$\overline{P_0Q_4} \perp \triangle P_1P_2P_3 \quad (2.46)$$

i.e., Q_4 is the perpendicular projection of P_0 on the plane containing $\triangle P_1P_2P_3$; (vii)

$$A_1 \stackrel{\text{def}}{=} A(\triangle P_2P_3P_4), \quad A_2 \stackrel{\text{def}}{=} A(\triangle P_3P_4P_1), \quad A_3 \stackrel{\text{def}}{=} A(\triangle P_4P_1P_2), \quad \text{and} \quad A_4 \stackrel{\text{def}}{=} A(\triangle P_1P_2P_3) \quad (2.47)$$

where $A(\triangle P_2P_3P_4)$, $A(\triangle P_3P_4P_1)$, $A(\triangle P_4P_1P_2)$, and $A(\triangle P_1P_2P_3)$ are the areas of the four triangular faces $\triangle P_2P_3P_4$, $\triangle P_3P_4P_1$, $\triangle P_4P_1P_2$, and $\triangle P_1P_2P_3$, respectively; (viii)

$$h_k \stackrel{\text{def}}{=} |\overline{P_0Q_k}| \quad k = 1, 2, 3, 4 \quad (2.48)$$

and (ix) the x - y - z coordinate system depicted in Fig. 6(a) is also a right-handed system which satisfies Eq. (2.8).

Note that, according to Eq. (2.47) and Fig. 6(a), for each $k = 1, 2, 3, 4$, A_k denotes the area of the face of the tetrahedron $P_1P_2P_3P_4$ which is opposite to the vertex P_k . Also from the definition of points Q_1 , Q_2 , Q_3 , and Q_4 and that of h_k , $k = 1, 2, 3, 4$, one concludes that h_1 , h_2 , h_3 , and h_4 , respectively, are the (shortest) distances from P_0 to the planes that contain the faces $\triangle P_2P_3P_4$, $\triangle P_3P_4P_1$, $\triangle P_4P_1P_2$, and $\triangle P_1P_2P_3$, respectively.

For each $k = 0, 1, 2, 3, 4$, let \vec{P}_k be the position vector of point P_k , i.e.,

$$\vec{P}_k \stackrel{\text{def}}{=} x_k \vec{e}_x + y_k \vec{e}_y + z_k \vec{e}_z \quad k = 0, 1, 2, 3, 4 \quad (2.49)$$

Also let \vec{P}_0 be an weighted average of \vec{P}_k , $k = 1, 2, 3, 4$, i.e.,

$$\vec{P}_0 = w_1 \vec{P}_1 + w_2 \vec{P}_2 + w_3 \vec{P}_3 + w_4 \vec{P}_4 \quad (2.50)$$

where w_1 , w_2 , w_3 , and w_4 are real weight factors with

$$w_1 + w_2 + w_3 + w_4 = 1 \quad (2.51)$$

Moreover, given a pair of integers k_1 and k_2 with $k_1 \neq k_2$ and $k_1, k_2 = 0, 1, 2, 3, 4$, let $\overrightarrow{P_{k_1}P_{k_2}}$ be the displacement vector joining points P_{k_1} and P_{k_2} and pointing in the direction from P_{k_1} to P_{k_2} , i.e.,

$$\overrightarrow{P_{k_1}P_{k_2}} \stackrel{\text{def}}{=} \vec{P}_{k_2} - \vec{P}_{k_1}, \quad k_1 \neq k_2 \quad \text{and} \quad k_1, k_2 = 0, 1, 2, 3, 4 \quad (2.52)$$

Then, by using Eq. (2.52) and other well-known properties of the vector product such as Eq. (2.13), one can show that Eq. (2.14) is still valid in the current 3D case. In turn, with the aid of Eqs. (2.14) and (2.52), and other well-known properties of the scalar triple product such as

$$(\vec{A} \times \vec{B}) \cdot \vec{C} = (\vec{B} \times \vec{C}) \cdot \vec{A} = (\vec{C} \times \vec{A}) \cdot \vec{B} = -(\vec{A} \times \vec{C}) \cdot \vec{B} \quad (2.53)$$

and

$$(\vec{A} \times \vec{A}) \cdot \vec{B} = (\vec{A} \times \vec{B}) \cdot \vec{A} = (\vec{B} \times \vec{A}) \cdot \vec{A} = 0 \quad (2.54)$$

for any vectors \vec{A} , \vec{B} , and \vec{C} , one can show that

$$\Delta \stackrel{\text{def}}{=} (\overrightarrow{P_1P_2} \times \overrightarrow{P_1P_3}) \cdot \overrightarrow{P_1P_4} = (\vec{P}_1 \times \vec{P}_2) \cdot \vec{P}_4 + (\vec{P}_2 \times \vec{P}_3) \cdot \vec{P}_4 + (\vec{P}_3 \times \vec{P}_1) \cdot \vec{P}_4 + (\vec{P}_3 \times \vec{P}_2) \cdot \vec{P}_1 \quad (2.55)$$

Moreover, by using Eqs. (2.13), (2.50) and (2.52), one has

$$\overrightarrow{P_0P_1} \times \overrightarrow{P_0P_2} = (1 - w_1 - w_2) \vec{P}_1 \times \vec{P}_2 + (w_3 \vec{P}_3 + w_4 \vec{P}_4) \times (\vec{P}_1 - \vec{P}_2) \quad (2.56)$$

Next, by using Eqs. (2.50)–(2.56), one can show that

$$\begin{aligned} & (\overrightarrow{P_0P_1} \times \overrightarrow{P_0P_2}) \cdot \overrightarrow{P_0P_3} \\ &= w_4 \left[(\vec{P}_1 \times \vec{P}_2) \cdot \vec{P}_3 + (\vec{P}_2 \times \vec{P}_1) \cdot \vec{P}_4 + (\vec{P}_3 \times \vec{P}_4) \cdot \vec{P}_1 + (\vec{P}_4 \times \vec{P}_3) \cdot \vec{P}_2 \right] = -w_4 \Delta \end{aligned} \quad (2.57)$$

In turn, by carrying out the index mapping

$$(1, 2, 3, 4) \rightarrow (2, 3, 4, 1)$$

of Eq. (2.57) repeatedly and using Eqs. (2.53)–(2.55), one obtains

$$\begin{aligned} & (\overrightarrow{P_0 P_2} \times \overrightarrow{P_0 P_3}) \cdot \overrightarrow{P_0 P_4} \\ &= w_1 \left[(\overrightarrow{P_2} \times \overrightarrow{P_3}) \cdot \overrightarrow{P_4} + (\overrightarrow{P_3} \times \overrightarrow{P_2}) \cdot \overrightarrow{P_1} + (\overrightarrow{P_4} \times \overrightarrow{P_1}) \cdot \overrightarrow{P_2} + (\overrightarrow{P_1} \times \overrightarrow{P_4}) \cdot \overrightarrow{P_3} \right] = w_1 \Delta \end{aligned} \quad (2.58)$$

$$\begin{aligned} & (\overrightarrow{P_0 P_3} \times \overrightarrow{P_0 P_4}) \cdot \overrightarrow{P_0 P_1} \\ &= w_2 \left[(\overrightarrow{P_3} \times \overrightarrow{P_4}) \cdot \overrightarrow{P_1} + (\overrightarrow{P_4} \times \overrightarrow{P_3}) \cdot \overrightarrow{P_2} + (\overrightarrow{P_1} \times \overrightarrow{P_2}) \cdot \overrightarrow{P_3} + (\overrightarrow{P_2} \times \overrightarrow{P_1}) \cdot \overrightarrow{P_4} \right] = -w_2 \Delta \end{aligned} \quad (2.59)$$

and

$$\begin{aligned} & (\overrightarrow{P_0 P_4} \times \overrightarrow{P_0 P_1}) \cdot \overrightarrow{P_0 P_2} \\ &= w_3 \left[(\overrightarrow{P_4} \times \overrightarrow{P_1}) \cdot \overrightarrow{P_2} + (\overrightarrow{P_1} \times \overrightarrow{P_4}) \cdot \overrightarrow{P_3} + (\overrightarrow{P_2} \times \overrightarrow{P_3}) \cdot \overrightarrow{P_4} + (\overrightarrow{P_3} \times \overrightarrow{P_2}) \cdot \overrightarrow{P_1} \right] = w_3 \Delta \end{aligned} \quad (2.60)$$

For any four different integers $k_1, k_2, k_3, k_4 = 0, 1, 2, 3, 4$, let

$$V(P_{k_1} P_{k_2} P_{k_3} P_{k_4}) \stackrel{\text{def}}{=} \text{the volume of the tetrahedron with the vertices } P_{k_1}, P_{k_2}, P_{k_3}, \text{ and } P_{k_4} \quad (2.61)$$

Then by using the definition of the scalar triple product along with Eqs. (2.55) and (2.57)–(2.60), one has

$$V(P_1 P_2 P_3 P_4) = |(\overrightarrow{P_1 P_2} \times \overrightarrow{P_1 P_3}) \cdot \overrightarrow{P_1 P_4}|/6 = |\Delta|/6 \quad (2.62)$$

$$V(P_0 P_2 P_3 P_4) = |(\overrightarrow{P_0 P_2} \times \overrightarrow{P_0 P_3}) \cdot \overrightarrow{P_0 P_4}|/6 = |w_1 \Delta|/6 = |w_1| \times V(P_1 P_2 P_3 P_4) \quad (2.63)$$

$$V(P_0 P_3 P_4 P_1) = |(\overrightarrow{P_0 P_3} \times \overrightarrow{P_0 P_4}) \cdot \overrightarrow{P_0 P_1}|/6 = |w_2 \Delta|/6 = |w_2| \times V(P_1 P_2 P_3 P_4) \quad (2.64)$$

$$V(P_0 P_4 P_1 P_2) = |(\overrightarrow{P_0 P_4} \times \overrightarrow{P_0 P_1}) \cdot \overrightarrow{P_0 P_2}|/6 = |w_3 \Delta|/6 = |w_3| \times V(P_1 P_2 P_3 P_4) \quad (2.65)$$

and

$$V(P_0 P_1 P_2 P_3) = |(\overrightarrow{P_0 P_1} \times \overrightarrow{P_0 P_2}) \cdot \overrightarrow{P_0 P_3}|/6 = |w_4 \Delta|/6 = |w_4| \times V(P_1 P_2 P_3 P_4) \quad (2.66)$$

Eqs. (2.63)–(2.66) \Rightarrow

$$\begin{aligned} & V(P_0 P_2 P_3 P_4) + V(P_0 P_3 P_4 P_1) + V(P_0 P_4 P_1 P_2) + V(P_0 P_1 P_2 P_3) \\ &= (|w_1| + |w_2| + |w_3| + |w_4|) \times V(P_1 P_2 P_3 P_4) \end{aligned} \quad (2.67)$$

Because the tetrahedron $P_1 P_2 P_3 P_4$ is intrinsically convex in the x - y - z space, point P_0 defined by Eqs. (2.50) and (2.51) lies on the boundary or in the interior of the tetrahedron $P_1 P_2 P_3 P_4 \Leftrightarrow$

$$0 \leq w_k \leq 1 \quad k = 1, 2, 3, 4 \quad (2.68)$$

Moreover, because Eq. (2.42) implies that the interior of the tetrahedron $P_1 P_2 P_3 P_4$ is not empty, P_0 lies in the interior of the tetrahedron $P_1 P_2 P_3 P_4 \Leftrightarrow$

$$0 < w_k < 1 \quad k = 1, 2, 3, 4 \quad (2.69)$$

For the case where P_0 lies on the boundary or in the interior of the tetrahedron $P_1 P_2 P_3 P_4$, Eqs. (2.51), (2.67), and (2.68) now \Rightarrow the following obvious result:

$$V(P_0 P_2 P_3 P_4) + V(P_0 P_3 P_4 P_1) + V(P_0 P_4 P_1 P_2) + V(P_0 P_1 P_2 P_3) = V(P_1 P_2 P_3 P_4) \quad (2.70)$$

On the other hand, for the case where P_0 lies outside of the tetrahedron $P_1P_2P_3P_4$, Eq. (2.68) is no longer true, i.e., some of the weight factors must be negative. Because Eq. (2.51) requires that some of the weight factors must be positive, we arrive at the conclusion that

$$|w_1| + |w_2| + |w_3| + |w_4| > |w_1 + w_2 + w_3 + w_4| = 1 \quad (2.71)$$

if P_0 lies outside of the tetrahedron $P_1P_2P_3P_4$. In turn, Eqs. (2.67) and (2.71) \Rightarrow

$$V(P_0P_2P_3P_4) + V(P_0P_3P_4P_1) + V(P_0P_4P_1P_2) + V(P_0P_1P_2P_3) > V(P_1P_2P_3P_4) \quad (2.72)$$

if P_0 lies outside of the tetrahedron $P_1P_2P_3P_4$.

Note that, for any real parameter ζ , Eqs. (2.42) and (2.47) \Rightarrow

$$A_k > 0 \quad \text{and} \quad (A_k)^\zeta > 0 \quad k = 1, 2, 3, 4; \quad -\infty < \zeta < +\infty \quad (2.73)$$

As such the weight factors

$$w_k(\zeta) \stackrel{\text{def}}{=} \frac{(A_k)^\zeta}{(A_1)^\zeta + (A_2)^\zeta + (A_3)^\zeta + (A_4)^\zeta} \quad k = 1, 2, 3, 4; \quad -\infty < \zeta < +\infty \quad (2.74)$$

are well defined and satisfy the conditions

$$0 < w_k(\zeta) < 1 \quad k = 1, 2, 3, 4 \quad -\infty < \zeta < +\infty \quad (2.75)$$

and

$$w_1(\zeta) + w_2(\zeta) + w_3(\zeta) + w_4(\zeta) = 1 \quad -\infty < \zeta < +\infty \quad (2.76)$$

Note that, even though the same notation is used, the weight factors $w_k(\zeta)$, $k = 1, 2, 3, 4$, defined in Eq. (2.74) are different from those defined in Eq. (2.29). The definition Eq. (2.74) will be used in this subsection.

Moreover, hereafter we consider only the special case where

$$w_k = w_k(\zeta) \quad k = 1, 2, 3, 4; \quad -\infty < \zeta < +\infty \quad (2.77)$$

For this special case, Eqs. (2.75)–(2.77) imply that both Eqs. (2.51) and (2.69) are satisfied for any real number ζ . Thus, for the case Eq. (2.77), (i) point P_0 defined by Eq. (2.50) must always lie in the interior of the tetrahedron $P_1P_2P_3P_4$, and (ii) Eqs. (2.63)–(2.67) reduce to

$$V(P_0P_2P_3P_4) = w_1 \times V(P_1P_2P_3P_4) \quad (2.78)$$

$$V(P_0P_3P_4P_1) = w_2 \times V(P_1P_2P_3P_4) \quad (2.79)$$

$$V(P_0P_4P_1P_2) = w_3 \times V(P_1P_2P_3P_4) \quad (2.80)$$

$$V(P_0P_1P_2P_3) = w_4 \times V(P_1P_2P_3P_4) \quad (2.81)$$

and Eq. (2.70), respectively. Moreover, for the special case $\zeta = 0$, we have

$$w_1 = w_2 = w_3 = w_4 = 1/4 \quad \text{and} \quad \vec{P}_0 = \left(\vec{P}_1 + \vec{P}_2 + \vec{P}_3 + \vec{P}_4 \right) / 4 \quad (\zeta = 0) \quad (2.82)$$

Because the position vector of the centroid of a tetrahedron is the simple average of those of its four vertices, Eq. (2.82) \Rightarrow point P_0 is the centroid of the tetrahedron $P_1P_2P_3P_4$ if $\zeta = 0$.

Note that, for a polyhedron other than a tetrahedron (which is the simplest polyhedron), generally it is not true that the position vector of its centroid is the simple average of those of its vertices. As an example,

the position vector of the centroid of a hexahedron may not be the simple average of those of its eight vertices unless the hexahedron is a parallelepiped.

Next, with the aid of Eq. (2.47) and (2.48), and Fig. 6(a), one can see that

$$V(P_0P_2P_3P_4) = \frac{h_1A_1}{3}, \quad V(P_0P_3P_4P_1) = \frac{h_2A_2}{3}, \quad V(P_0P_4P_1P_2) = \frac{h_3A_3}{3} \quad \text{and} \quad V(P_0P_1P_2P_3) = \frac{h_4A_4}{3} \quad (2.83)$$

In turn, by substituting Eq. (2.83) into Eqs. (2.78)–(2.81) and using Eqs. (2.74) and (2.77), one has

$$\frac{h_kA_k}{3} = w_kV(P_1P_2P_3P_4) = \frac{(A_k)^\zeta \times V(P_1P_2P_3P_4)}{(A_1)^\zeta + (A_2)^\zeta + (A_3)^\zeta + (A_4)^\zeta} \quad k = 1, 2, 3, 4; \quad -\infty < \zeta < +\infty \quad (2.84)$$

and thus

$$\frac{h_1}{(A_1)^{\zeta-1}} = \frac{h_2}{(A_2)^{\zeta-1}} = \frac{h_3}{(A_3)^{\zeta-1}} = \frac{h_4}{(A_4)^{\zeta-1}} = \frac{3 \times V(P_1P_2P_3P_4)}{(A_1)^\zeta + (A_2)^\zeta + (A_3)^\zeta + (A_4)^\zeta} \quad -\infty < \zeta < +\infty \quad (2.85)$$

Because (i) $h_1, h_2, h_3,$ and h_4 are the distances from point P_0 to the triangular faces $\triangle P_2P_3P_4, \triangle P_3P_4P_1, \triangle P_4P_1P_2,$ and $\triangle P_1P_2P_3$ respectively, and (ii) $A_1, A_2, A_3,$ and A_4 are the areas of $\triangle P_2P_3P_4, \triangle P_3P_4P_1, \triangle P_4P_1P_2,$ and $\triangle P_1P_2P_3,$ respectively, Eq. (2.85) states that, for a given tetrahedron $P_1P_2P_3P_4$ and a given $\zeta,$ the distance from point P_0 to any face of this tetrahedron is proportional to the $(\zeta - 1)$ th power of the area of the face.

In fact, for the case $\zeta = 0$ (i.e., when P_0 is the centroid of the tetrahedron $P_1P_2P_3P_4$), Eq. (2.85) reduces to

$$h_k = \left[\frac{3 \times V(P_1P_2P_3P_4)}{4} \right] \frac{1}{A_k} \quad k = 1, 2, 3, 4, \quad \text{if } \zeta = 0 \quad (2.86)$$

i.e., the distance between the centroid P_0 and a face of the tetrahedron $P_1P_2P_3P_4$ is inversely proportional to the area of this face. Thus the centroid is farthest away from the smallest face and closest to the largest face.

On the other hand, for the case $\zeta = 1,$ Eq. (2.85) reduces to

$$h_1 = h_2 = h_3 = h_4 = \frac{3 \times V(P_1P_2P_3P_4)}{A_1 + A_2 + A_3 + A_4} \quad \text{if } \zeta = 1 \quad (2.87)$$

i.e., point P_0 has the same distance to the four faces of the tetrahedron $P_1P_2P_3P_4$ if $\zeta = 1.$ By definition, this implies that P_0 is the *in-center* of the tetrahedron $P_1P_2P_3P_4$ for the case $\zeta = 1.$

In general one can infer from Eq. (2.85) that:

- (a) For the case $\zeta > 1,$ point P_0 is farthest away from the largest face of the tetrahedron $P_1P_2P_3P_4$ and closest to its smallest face. The trend becomes stronger as the value of ζ increases from 1.
- (b) For the case $\zeta < 1,$ point P_0 is farthest away from the smallest face of the tetrahedron $P_1P_2P_3P_4$ and closest to its largest face. The trend becomes stronger as the value of ζ decreases from 1.

Let the interior point P_0 of any tetrahedron $P_1P_2P_3P_4$ defined by Eqs. (2.50) and (2.77) be referred to as the *interior point of this tetrahedron associated with the parameter $\zeta.$* Then, from the above observations and the discussions given in Sec. 1, it becomes clear that a *spatial solution point which is the centroid of the 8-vertex polyhedron referred to earlier will be much less likely to lie outside of the associated 8-vertex polyhedron and causes numerical difficulties if each of the centroidal mesh points P_0, A_0, B_0, C_0 and D_0 depicted in Fig. 6(b) is replaced by an interior point associated with a parameter $\zeta \geq 1.$ In fact, it has been shown through numerical experiments that the numerical difficulties associated with spatial solution points being embedded beyond a solid-wall boundary can be overcome by replacing centroids of tetrahedra with in-centers (i.e., interior points associated with $\zeta = 1$) in the construction of a spatial tetrahedral mesh.*

3. Flux-conserving solution-coupling procedures

In this section, it will be described how an 1D CESE scheme can be modified so that the two decoupled solutions of the original scheme can become coupled in the new scheme while still preserving a flux conservation condition to be defined shortly. This description is then followed by a sketch of the 2D and 3D extensions.

3.1. 1D CESE solution-coupling schemes

As a preliminary, note that the CEs, SEs and the 1D schemes, which were defined over Ω_1 in Sec. 1, hereafter will be defined over

$$\Omega \stackrel{\text{def}}{=} \{(j, n) | j, n = 0, \pm 1/2, \pm 1, \pm 3/2, \dots\} = \Omega_1 \cup \Omega_2 \quad (3.1)$$

In particular, *it should be understood that the symbol Ω_1 from now on is replaced by Ω in each of Eqs. (1.3)–(1.16)*. Also, as an example, the extension (defined over Ω) of the a - ϵ scheme will be referred to as the dual a - ϵ scheme.

To clarify the significance of the extension, we offer the following observations:

- (a) The solution of a dual scheme is formed by two decoupled solutions which are defined over Ω_1 and Ω_2 , respectively.
- (b) The same space-time region can be designated as a BCE of a mesh point $\in \Omega_1$ and also as a BCE of another mesh point $\in \Omega_2$. For examples, the space-time region $ABCD$ depicted in Fig. 2(c) can be designated as $\text{CE}_-(j, n)$ and $\text{CE}_+(j - 1/2, n)$, respectively, while the region $AFED$ depicted in Fig. 2(d) as $\text{CE}_+(j, n)$ and $\text{CE}_-(j + 1/2, n)$, respectively. Hereafter, as an example, *points (j, n) and $(j - 1/2, n)$ (i.e., points A and B) will be referred to as the hosts of the region $ABCD$* .
- (c) Let the region $ABCD$ be designated as $\text{CE}_-(j, n)$. Then, on its boundary, the line segments \overline{AB} and \overline{AD} belong to $\text{SE}(j, n)$ while \overline{CB} and \overline{CD} belong to $\text{SE}(j - 1/2, n - 1/2)$, i.e., over \overline{AB} and \overline{AD} , the vector \vec{h}^* should be evaluated using the solution data stored at point A while, over \overline{CB} and \overline{CD} , it should be evaluated using those stored at point C .

Alternately, let the region $ABCD$ be designated as $\text{CE}_+(j - 1/2, n)$. Then, on its boundary, the line segments \overline{BA} and \overline{BC} belong to $\text{SE}(j - 1/2, n)$ while \overline{DA} and \overline{DC} belong to $\text{SE}(j, n - 1/2)$, i.e., over \overline{BA} and \overline{BC} , the vector \vec{h}^* should be evaluated using the solution data stored at point B while, over \overline{DA} and \overline{DC} , it should be evaluated using those stored at point D . Note that, *in the above and hereafter, as an example, a line segment joining points A and B is denoted by \overline{AB} if it belongs to $\text{SE}(A)$ (i.e., the SE centered at point A) while the same line segment is denoted by \overline{BA} if it belongs $\text{SE}(B)$ (i.e., the SE centered at point B)*.

- (d) From the discussions given in the above item (c), it becomes clear that

$$\oint_{S(\text{CE}_+(j, n))} \vec{h}^* \cdot d\vec{s} = 0 \quad \text{and} \quad \oint_{S(\text{CE}_-(j+1/2, n))} \vec{h}^* \cdot d\vec{s} = 0 \quad (j, n) \in \Omega \quad (3.2)$$

represent two different flux conservation conditions even though $\text{CE}_+(j, n)$ and $\text{CE}_-(j + 1/2, n)$ occupy the same space-time region for any $(j, n) \in \Omega$.

As will be shown, each marching step of the 1D solution-coupling scheme is formed by two sub-steps. In the first sub-step, referred to as the dual-scheme marching step, the intermediate mesh values at the n th time level are evaluated from the given mesh values at the $(n - 1/2)$ th time level using a dual-scheme (see Fig. 7). In the second sub-step, referred to as the solution-coupling step, the final mesh values at the n th time level are updated from the intermediate mesh values through a flux-conserving weighted-averaging procedure. Let the intermediate mesh values of u and its normalized spatial derivative $u_{\bar{x}}$ at any $(j, n) \in \Omega$ be denoted by \hat{u}_j^n and $(\hat{u}_{\bar{x}})_j^n$, respectively. Then, as an example, \hat{u}_j^n and $(\hat{u}_{\bar{x}})_j^n$ can be evaluated in terms of the given mesh values at the $(n - 1/2)$ th time level by using the dual a - ϵ scheme defined by Eqs. (1.12) and (1.15), i.e.,

$$\hat{u}_j^n = \frac{1}{2} \left\{ (1 - \nu) [u - (1 + \nu)u_{\bar{x}}]_{j+1/2}^{n-1/2} + (1 + \nu) [u + (1 - \nu)u_{\bar{x}}]_{j-1/2}^{n-1/2} \right\} \quad (j, n) \in \Omega \quad (3.3)$$

and

$$(\hat{u}_{\bar{x}})_j^n = \frac{1}{2} \left\{ [(1-\epsilon)u + (2\epsilon-1-\nu)u_{\bar{x}}]_{j+1/2}^{n-1/2} - [(1-\epsilon)u + (1-\nu-2\epsilon)u_{\bar{x}}]_{j-1/2}^{n-1/2} \right\} \quad (j, n) \in \Omega \quad (3.4)$$

Note that, by using a relation similar to the second equation in Eq. (1.9), one can define the “unnormalized” version of $(\hat{u}_{\bar{x}})_j^n$, i.e.,

$$(\hat{u}_x)_j^n \stackrel{\text{def}}{=} \frac{4}{\Delta x} (\hat{u}_{\bar{x}})_j^n \quad (j, n) \in \Omega \quad (3.5)$$

To avoid introducing unnecessary new notations, in the following description of the solution-coupling step, at each $(j, n) \in \Omega$, the final mesh values after updating from the intermediate values are simply denoted as u_j^n and $(u_{\bar{x}})_j^n$, respectively.

Note that the line segment \overline{AF} depicted in Fig. 7 belongs to $\text{SE}(j, n)$. Thus, by using (i) Eqs. (1.4), (1.6) and (1.9), and (ii) Fig. 2(d), one concludes that the flux of \vec{h}^* leaving $\text{CE}_+(j, n)$ through \overline{AF} evaluated using the final solution data stored at point A is given by

$$F(\overline{AF}) \stackrel{\text{def}}{=} \int_{x_j}^{x_j+(\Delta x/2)} u^*(x, t^n; j, n) dx = \frac{\Delta x}{2} (u_+)_j^n \quad (j, n) \in \Omega \quad (3.6)$$

where

$$(u_+)_j^n \stackrel{\text{def}}{=} (u + u_{\bar{x}})_j^n \quad (j, n) \in \Omega \quad (3.7)$$

Let $\hat{F}(\overline{AF})$ be the intermediate value of $F(\overline{AF})$, i.e., the value of $F(\overline{AF})$ when u_j^n and $(u_{\bar{x}})_j^n$ are replaced by \hat{u}_j^n and $(\hat{u}_{\bar{x}})_j^n$, respectively. Then Eqs. (3.5)–(3.7) \Rightarrow

$$\hat{F}(\overline{AF}) = \frac{\Delta x}{2} (\hat{u}_+)_j^n \quad (j, n) \in \Omega \quad (3.8)$$

where

$$(\hat{u}_+)_j^n \stackrel{\text{def}}{=} (\hat{u} + \hat{u}_{\bar{x}})_j^n \quad (j, n) \in \Omega \quad (3.9)$$

At this juncture, note that: (i) at the midpoint M_+ of \overline{AF} , $x = x_j + (\Delta x/4)$ and $t = t^n$; and (ii) Eqs. (1.6), (1.9), and (3.7) \Rightarrow

$$u^*(x_j + (\Delta x/4), t^n; j, n) = (u_+)_j^n \quad (j, n) \in \Omega \quad (3.10)$$

Thus, $(u_+)_j^n$ is the value of u at the midpoint M_+ of \overline{AF} evaluated using the values u_j^n and $(u_{\bar{x}})_j^n$ with the aid of Eqs. (1.6) and (1.9). Similarly $(\hat{u}_+)_j^n$ is the value of u at the midpoint M_+ evaluated using the intermediate values \hat{u}_j^n and $(\hat{u}_{\bar{x}})_j^n$ with the aid of Eqs. (1.6), (1.9), and (3.5).

Because $(u_+)_j^n$ and $(\hat{u}_+)_j^n$ are evaluated using the solution data stored at point (j, n) (i.e., point A), hereafter, respectively, they will be referred to as the final and intermediate values of u at the midpoint M_+ associated with the host point A of the region $AFED$. Similarly, $F(\overline{AF})$ and $\hat{F}(\overline{AF})$, respectively, are referred to as the final and intermediate values of the flux leaving the top face of the same region associated with the same host.

Moreover, with the aid of Eqs. (3.6) and (3.8), and Fig. 7, one concludes that $F(\overline{AF})$ ($\hat{F}(\overline{AF})$) is equal to the length of \overline{AF} multiplied by the approximated value $(u_+)_j^n$ ($(\hat{u}_+)_j^n$) of u at the midpoint M_+ . In other words, the value of u at the midpoint M_+ is the average value of u over \overline{AF} —a result stemmed from the fact that $u^*(x, t; j, n)$ is a first-order Taylor’s expansion in x when $t = t^n$ (see Eqs. (1.3) and (1.6)).

Similarly, with the aid of Fig. 7, one concludes that:

- (a) The flux of \vec{h}^* leaving $\text{CE}_-(j, n)$ through the line segment \overline{AB} evaluated using the final solution data stored at point A is given by

$$F(\overline{AB}) \stackrel{\text{def}}{=} \int_{x_j}^{x_j-(\Delta x/2)} u^*(x, t^n; j, n) dx = \frac{\Delta x}{2} (u_-)_j^n \quad (j, n) \in \Omega \quad (3.11)$$

where

$$(u_-)_j^n \stackrel{\text{def}}{=} (u - u_{\bar{x}})_j^n \quad (j, n) \in \Omega \quad (3.12)$$

is the value of u at the midpoint M_- of \overline{AB} evaluated using the values u_j^n and $(u_{\bar{x}})_j^n$ with the aid of Eqs. (1.6) and (1.9).

Also $\hat{F}(\overline{AB})$, the intermediate value of $F(\overline{AB})$, is given by

$$\hat{F}(\overline{AB}) = \frac{\Delta x}{2} (\hat{u}_-)_j^n \quad (j, n) \in \Omega \quad (3.13)$$

where

$$(\hat{u}_-)_j^n \stackrel{\text{def}}{=} (\hat{u} - \hat{u}_{\bar{x}})_j^n \quad (j, n) \in \Omega \quad (3.14)$$

is the value of u at the midpoint M_- evaluated using the intermediate values \hat{u}_j^n and $(\hat{u}_{\bar{x}})_j^n$ with the aid of Eqs. (1.6), (1.9), and (3.5).

Because $(u_-)_j^n$ and $(\hat{u}_-)_j^n$ are evaluated using the solution data stored at point (j, n) (i.e., point A), hereafter, respectively, they will be referred to as the final and intermediate values of u at the midpoint M_- associated with the host point A of the region $ABCD$. Similarly, $F(\overline{AB})$ and $\hat{F}(\overline{AB})$, respectively, are referred to as the final and intermediate values of the flux leaving the top face of the same region associated with the same host.

Moreover, with the aid of Eqs. (3.11) and (3.13), one concludes that $F(\overline{AB})$ ($\hat{F}(\overline{AB})$) is equal to the length of \overline{AB} multiplied by the approximated value $(u_-)_j^n$ ($(\hat{u}_-)_j^n$) of u at the midpoint M_- .

- (b) The flux of \vec{h}^* leaving $\text{CE}_-(j + 1/2, n)$ through the line segment \overline{FA} evaluated using the final solution data stored at point F is given by

$$F(\overline{FA}) \stackrel{\text{def}}{=} \int_{x_j}^{x_j + (\Delta x/2)} u^*(x, t^n; j + 1/2, n) dx = \frac{\Delta x}{2} (u_-)_{j+1/2}^n \quad (j, n) \in \Omega \quad (3.15)$$

where

$$(u_-)_{j+1/2}^n \stackrel{\text{def}}{=} (u - u_{\bar{x}})_{j+1/2}^n \quad (j, n) \in \Omega \quad (3.16)$$

is the value of u at the midpoint M_+ of \overline{FA} evaluated using the values $u_{j+1/2}^n$ and $(u_{\bar{x}})_{j+1/2}^n$ with the aid of Eqs. (1.6) and (1.9). Note that: (i) because $(j, n) \in \Omega \Leftrightarrow (j + 1/2, n) \in \Omega$, Eq. (3.12) \Leftrightarrow Eq. (3.16); and (ii) according to Eqs. (3.6) and (3.15), $F(\overline{AF}) \neq F(\overline{FA})$ even though \overline{AF} and \overline{FA} denote the same line segment. In fact, $F(\overline{AF})$ is a flux evaluated using the solution data stored at point A while $F(\overline{FA})$ is another flux evaluated using those stored at point F . The reader is warned that other similar pairs of notations will appear throughout the paper.

Also $\hat{F}(\overline{FA})$, the intermediate value of $F(\overline{FA})$, is given by

$$\hat{F}(\overline{FA}) = \frac{\Delta x}{2} (\hat{u}_-)_{j+1/2}^n \quad (j, n) \in \Omega \quad (3.17)$$

where

$$(\hat{u}_-)_{j+1/2}^n \stackrel{\text{def}}{=} (\hat{u} - \hat{u}_{\bar{x}})_{j+1/2}^n \quad (j, n) \in \Omega \quad (3.18)$$

is the value of u at the midpoint M_+ evaluated using the intermediate values $\hat{u}_{j+1/2}^n$ and $(\hat{u}_{\bar{x}})_{j+1/2}^n$ with the aid of Eqs. (1.6), (1.9), and (3.5). Obviously Eq. (3.14) \Leftrightarrow Eq. (3.18).

Because $(u_-)_{j+1/2}^n$ and $(\hat{u}_-)_{j+1/2}^n$ are evaluated using the solution data stored at point $(j + 1/2, n)$ (i.e., point F), hereafter, respectively, they will be referred to as the final and intermediate values of u at the midpoint M_+ associated with the host point F of the region $AFED$. Similarly, $F(\overline{FA})$ and $\hat{F}(\overline{FA})$, respectively, are referred to as the final and intermediate values of the flux leaving the top face of the same region associated with the same host.

Moreover, with the aid of Eqs. (3.15) and (3.17), one concludes that $F(\overline{FA})$ ($\hat{F}(\overline{FA})$) is equal to the length of \overline{FA} multiplied by the approximated value $(u_-)_{j+1/2}^n$ ($(\hat{u}_-)_{j+1/2}^n$) of u at the midpoint M_+ .

- (c) The flux of \vec{h}^* leaving $CE_+(j-1/2, n)$ through the line segment \overline{BA} evaluated using the final solution data stored at point B is given by

$$F(\overline{BA}) \stackrel{\text{def}}{=} \int_{x_j - (\Delta x/2)}^{x_j} u^*(x, t^n; j-1/2, n) dx = \frac{\Delta x}{2} (u_+)_{j-1/2}^n \quad (j, n) \in \Omega \quad (3.19)$$

where

$$(u_+)_{j-1/2}^n \stackrel{\text{def}}{=} (u + u_{\bar{x}})_{j-1/2}^n \quad (j, n) \in \Omega \quad (3.20)$$

is the value of u at the midpoint M_- of \overline{BA} evaluated using the values $u_{j-1/2}^n$ and $(u_{\bar{x}})_{j-1/2}^n$ with the aid of Eqs. (1.6) and (1.9). Obviously, Eq. (3.7) \Leftrightarrow Eq. (3.20).

Also $\hat{F}(\overline{BA})$, the intermediate value of $F(\overline{BA})$, is given by

$$\hat{F}(\overline{BA}) = \frac{\Delta x}{2} (\hat{u}_+)_{j-1/2}^n \quad (j, n) \in \Omega \quad (3.21)$$

where

$$(\hat{u}_+)_{j-1/2}^n \stackrel{\text{def}}{=} (\hat{u} + \hat{u}_{\bar{x}})_{j-1/2}^n \quad (j, n) \in \Omega \quad (3.22)$$

is the value of u at the midpoint M_- evaluated using the intermediate values $\hat{u}_{j-1/2}^n$ and $(\hat{u}_{\bar{x}})_{j-1/2}^n$ with the aid of Eqs. (1.6), (1.9), and (3.5). Obviously Eq. (3.9) \Leftrightarrow Eq. (3.22).

Because $(u_+)_{j-1/2}^n$ and $(\hat{u}_+)_{j-1/2}^n$ are evaluated using the solution data stored at point $(j-1/2, n)$ (i.e., point B), hereafter, respectively, they will be referred to as the final and intermediate values of u at the midpoint M_- associated with the host point B of the region $ABCD$. Similarly, $F(\overline{BA})$ and $\hat{F}(\overline{BA})$, respectively, are referred to as the final and intermediate values of the flux leaving the top face of the same region associated with the same host.

Moreover, with the aid of Eqs. (3.19) and (3.21), one concludes that $F(\overline{BA})$ ($\hat{F}(\overline{BA})$) is equal to the length of \overline{BA} multiplied by the approximated value $(u_+)_{j-1/2}^n$ ($(\hat{u}_+)_{j-1/2}^n$) of u at the midpoint M_- .

Next recall that two different final fluxes $F(\overline{AF})$ and $F(\overline{FA})$, respectively associated with the host points A and F of the region $AFED$, are defined over the top face of this region. For a reason explained in [42], the dual flux (denoted by $F(A; F)$ or $F(F; A)$) associated with these two fluxes is defined as the simple average of them, i.e.,

$$F(A; F) \equiv F(F; A) \stackrel{\text{def}}{=} [F(\overline{AF}) + F(\overline{FA})] / 2 \quad (3.23)$$

Similarly, we have

$$\hat{F}(A; F) \equiv \hat{F}(F; A) \stackrel{\text{def}}{=} [\hat{F}(\overline{AF}) + \hat{F}(\overline{FA})] / 2 \quad (3.24)$$

The solution-coupling step will be constructed so that, at the top face of any BCE (such as the space-time region $AFED$) sandwiched between the n th and $(n-1/2)$ th time levels, the dual flux evaluated using u_j^n and $(u_{\bar{x}})_j^n$, $(j, n) \in \Omega$, is equal to that evaluated using \hat{u}_j^n and $(\hat{u}_{\bar{x}})_j^n$, $(j, n) \in \Omega$, i.e.,

$$F(A; F) = \hat{F}(A; F) \quad (j, n) \in \Omega \quad (3.25)$$

By substituting Eqs. (3.6), (3.8), (3.15), and (3.17) into Eqs. (3.23) and (3.24), and then imposing the condition Eq. (3.25), one has

$$(u_+)_{j-1/2}^n + (u_-)_{j+1/2}^n = (\hat{u}_+)_{j-1/2}^n + (\hat{u}_-)_{j+1/2}^n \quad (j, n) \in \Omega \quad (3.26)$$

Recall that: (i) $(u_+)_{j-1/2}^n$ and $(u_-)_{j+1/2}^n$, respectively, are the final values of u at the midpoint M_+ evaluated using the solution data stored at the two hosts (points A and F) of the region $AFED$; and (ii) $(\hat{u}_+)_{j-1/2}^n$ and

$(\hat{u}_-)^n_{j+1/2}$, respectively, are the intermediate-value counterparts of $(u_+)^n_j$ and $(u_-)^n_{j+1/2}$. As such, Eq. (3.26) states that *the average of the two final values of u at the midpoint M_+ evaluated, respectively, using the solution data stored at the two hosts of the region AFED, is identical to its intermediate-value counterpart.*

Let

$$(u_+)^n_j = (1 - \eta)(\hat{u}_+)^n_j + \eta(\hat{u}_-)^n_{j+1/2} \quad (j, n) \in \Omega \quad (3.27)$$

where η is a real adjustable parameter. Then $(u_+)^n_j$ is an weighted average of $(\hat{u}_+)^n_j$ and $(\hat{u}_-)^n_{j+1/2}$. In turn, by substituting Eq. (3.27) into Eq. (3.26), one has

$$(u_-)^n_{j+1/2} = \eta(\hat{u}_+)^n_j + (1 - \eta)(\hat{u}_-)^n_{j+1/2} \quad (j, n) \in \Omega \quad (3.28)$$

i.e., $(u_-)^n_{j+1/2}$ is also an weighted average of $(\hat{u}_+)^n_j$ and $(\hat{u}_-)^n_{j+1/2}$. In fact, Eqs. (3.27) and (3.28) \Rightarrow (i)

$$(u_+)^n_j = (\hat{u}_+)^n_j \quad \text{and} \quad (u_-)^n_{j+1/2} = (\hat{u}_-)^n_{j+1/2} \quad \text{if} \quad \eta = 0 \quad (j, n) \in \Omega \quad (3.29)$$

(ii)

$$(u_+)^n_j = (u_-)^n_{j+1/2} = \frac{1}{2} \left[(\hat{u}_+)^n_j + (\hat{u}_-)^n_{j+1/2} \right] \quad \text{if} \quad \eta = 1/2 \quad (j, n) \in \Omega \quad (3.30)$$

and (iii)

$$(u_+)^n_j = (\hat{u}_-)^n_{j+1/2} \quad \text{and} \quad (u_-)^n_{j+1/2} = (\hat{u}_+)^n_j \quad \text{if} \quad \eta = 1 \quad (j, n) \in \Omega \quad (3.31)$$

Because $(j, n) \in \Omega \Leftrightarrow (j - 1/2, n) \in \Omega$, Eq. (3.27)–(3.31) remain valid if each index j in these equations is replaced by $j - 1/2$. In particular, Eq. (3.28) \Leftrightarrow

$$(u_-)^n_j = \eta(\hat{u}_+)^n_{j-1/2} + (1 - \eta)(\hat{u}_-)^n_j \quad (j, n) \in \Omega \quad (3.32)$$

In turn, by substituting Eqs. (3.7), (3.9), (3.12), (3.14), (3.18), and (3.22) into Eqs.(3.27) and (3.32), one has

$$(u + u_{\bar{x}})^n_j = (1 - \eta)(\hat{u} + \hat{u}_{\bar{x}})^n_j + \eta(\hat{u} - \hat{u}_{\bar{x}})^n_{j+1/2} \quad (j, n) \in \Omega \quad (3.33)$$

$$(u - u_{\bar{x}})^n_j = (1 - \eta)(\hat{u} - \hat{u}_{\bar{x}})^n_j + \eta(\hat{u} + \hat{u}_{\bar{x}})^n_{j-1/2} \quad (j, n) \in \Omega \quad (3.34)$$

By adding Eqs. (3.33) and (3.34) together, one has

$$u_j^n = (1 - \eta)\hat{u}_j^n + (\eta/2) \left[(\hat{u} - \hat{u}_{\bar{x}})^n_{j+1/2} + (\hat{u} + \hat{u}_{\bar{x}})^n_{j-1/2} \right] \quad (j, n) \in \Omega \quad (3.35)$$

On the other hand, by subtracting Eq. (3.34) from Eq. (3.33), one has

$$(u_{\bar{x}})^n_j = (1 - \eta)(\hat{u}_{\bar{x}})^n_j + (\eta/2) \left[(\hat{u} - \hat{u}_{\bar{x}})^n_{j+1/2} - (\hat{u} + \hat{u}_{\bar{x}})^n_{j-1/2} \right] \quad (j, n) \in \Omega \quad (3.36)$$

Eqs. (3.35) and (3.36) form the solution coupling step, i.e., with the aid of these two equations, at each mesh point $(j, n) \in \Omega$, u_j^n and $(u_{\bar{x}})^n_j$ can be determined in terms of the intermediate mesh values at the mesh points $(j - 1/2, n)$, (j, n) , and $(j + 1/2, n)$.

As expected from Eq. (3.29), we have

$$u_j^n = \hat{u}_j^n \quad \text{and} \quad (u_{\bar{x}})^n_j = (\hat{u}_{\bar{x}})^n_j \quad \text{if} \quad \eta = 0 \quad (j, n) \in \Omega \quad (3.37)$$

i.e., solution coupling does not occur when $\eta = 0$. On the other hand, because of Eq. (3.30), the case with $\eta = 1/2$ is referred as the full coupling case.

Let the dual-scheme marching step be executed using the a - ϵ scheme, i.e., Eqs. (3.3) and (3.4) are assumed. Then, by substituting Eqs. (3.3) and (3.4) into Eqs. (3.35) and (3.36), one obtains

$$\begin{aligned}
u_j^n &= \frac{\eta}{2} [(2 - \epsilon)u - \nu u_{\bar{x}}]_j^{n-1/2} \\
&+ \frac{(1 - \eta)}{2} \left\{ [(1 + \nu)u + (1 - \nu^2)u_{\bar{x}}]_{j-1/2}^{n-1/2} + [(1 - \nu)u - (1 - \nu^2)u_{\bar{x}}]_{j+1/2}^{n-1/2} \right\} \\
&+ \frac{\eta}{4} \left\{ [(\epsilon + \nu)u + (2\epsilon + \nu - \nu^2)u_{\bar{x}}]_{j-1}^{n-1/2} + [(\epsilon - \nu)u + (\nu + \nu^2 - 2\epsilon)u_{\bar{x}}]_{j+1}^{n-1/2} \right\}
\end{aligned} \quad (j, n) \in \Omega \quad (3.38)$$

and

$$\begin{aligned}
(u_{\bar{x}})_j^n &= \frac{\eta}{2} [\nu u + (2 - 2\epsilon - \nu^2)u_{\bar{x}}]_j^{n-1/2} \\
&+ \frac{(1 - \eta)}{2} \left\{ [(\epsilon - 1)u + (2\epsilon - 1 + \nu)u_{\bar{x}}]_{j-1/2}^{n-1/2} + [(1 - \epsilon)u + (2\epsilon - 1 - \nu)u_{\bar{x}}]_{j+1/2}^{n-1/2} \right\} \\
&- \frac{\eta}{4} \left\{ [(\epsilon + \nu)u + (2\epsilon + \nu - \nu^2)u_{\bar{x}}]_{j-1}^{n-1/2} - [(\epsilon - \nu)u + (\nu + \nu^2 - 2\epsilon)u_{\bar{x}}]_{j+1}^{n-1/2} \right\}
\end{aligned} \quad (j, n) \in \Omega \quad (3.39)$$

Because Eqs. (3.38) and (3.39) are derived assuming that (i) the dual-mesh marching step is carried out using the dual a - ϵ scheme, and (ii) the solution-coupling step is formed using an weighted-averaging procedure involving the parameter η (see Eq. (3.27)), hereafter the full solution-coupling scheme formed by Eqs. (3.38) and (3.39) will be referred to as the a - ϵ - η scheme.

Alternatively, the dual marching step can be executed using the dual c - τ scheme which are defined by Eqs. (1.12) and (1.16). For this case, the intermediate values \hat{u}_j^n and $(\hat{u}_{\bar{x}})_j^n$ should be evaluated using Eq. (3.3) and

$$(\hat{u}_{\bar{x}})_j^n = \frac{1}{2(1 + \tau)} \left\{ [u - (1 + 2\nu - \tau)u_{\bar{x}}]_{j+1/2}^{n-1/2} - [u + (1 - 2\nu - \tau)u_{\bar{x}}]_{j-1/2}^{n-1/2} \right\} \quad (j, n) \in \Omega \quad (3.40)$$

By substituting Eqs. (3.3) and (3.40) into Eqs. (3.35) and (3.36), one obtains the c - τ - η scheme, i.e.,

$$\begin{aligned}
u_j^n &= \frac{\eta}{2(1 + \tau)} [(2 + \tau)u - 2\nu u_{\bar{x}}]_j^{n-1/2} \\
&+ \frac{(1 - \eta)}{2} \left\{ [(1 + \nu)u + (1 - \nu^2)u_{\bar{x}}]_{j-1/2}^{n-1/2} + [(1 - \nu)u - (1 - \nu^2)u_{\bar{x}}]_{j+1/2}^{n-1/2} \right\} \\
&+ \frac{\eta}{4(1 + \tau)} \left\{ [(\tau + \nu + \tau\nu)u + [2(\nu + \tau) - (1 + \tau)\nu^2]u_{\bar{x}}]_{j-1}^{n-1/2} \right. \\
&\left. + [(\tau - \nu - \tau\nu)u + [2(\nu - \tau) + (1 + \tau)\nu^2]u_{\bar{x}}]_{j+1}^{n-1/2} \right\}
\end{aligned} \quad (j, n) \in \Omega \quad (3.41)$$

and

$$\begin{aligned}
(u_{\bar{x}})_j^n &= \frac{\eta}{2(1 + \tau)} [(1 + \tau)\nu u + [2 - (1 + \tau)\nu^2]u_{\bar{x}}]_j^{n-1/2} \\
&- \frac{(1 - \eta)}{2(1 + \tau)} \left\{ [u + (1 - 2\nu - \tau)u_{\bar{x}}]_{j-1/2}^{n-1/2} - [u - (1 + 2\nu - \tau)u_{\bar{x}}]_{j+1/2}^{n-1/2} \right\} \\
&- \frac{\eta}{4(1 + \tau)} \left\{ [(\tau + \nu + \tau\nu)u + [2(\nu + \tau) - (1 + \tau)\nu^2]u_{\bar{x}}]_{j-1}^{n-1/2} \right. \\
&\left. - [(\tau - \nu - \tau\nu)u + [2(\nu - \tau) + (1 + \tau)\nu^2]u_{\bar{x}}]_{j+1}^{n-1/2} \right\}
\end{aligned} \quad (j, n) \in \Omega \quad (3.42)$$

The von Neumann stability analysis was carried out for both a - ϵ - η and c - τ - η scheme. In particular, the amplification matrices and the associated amplification factors were obtained for both schemes involving arbitrary values of ϵ , τ , η , and the phase angle θ [72]. Because the a - ϵ - η and c - τ - η schemes reduce to the dual a - ϵ and c - τ schemes, respectively when $\eta = 0$, as expected, the stability conditions of these two schemes also reduce to those of the a - ϵ and c - τ schemes, respectively when $\eta = 0$. For the general case involving an arbitrary value of η , it turns out that the stability conditions of these schemes generally become so complicated that they can only be expressed numerically. As such, the discussion of their stability conditions for the general case is beyond the scope of the current paper.

However, for the full coupling case, i.e., when $\eta = 1/2$, it can be shown that [72] the a - ϵ - η scheme is von Neumann stable \Leftrightarrow

$$\nu^4 \leq \epsilon \leq 1 \quad (\text{the } a\text{-}\epsilon\text{-}\eta \text{ scheme with } \eta = 1/2) \quad (3.43)$$

Let

$$\epsilon = \beta |\nu| \quad \beta > 0 \quad (3.44)$$

where $\beta > 0$ is an adjustable parameter. Then Eq. (3.43) becomes

$$\nu^4 \leq \beta |\nu| \leq 1 \quad (3.45)$$

Excluding the meaningless case $\nu = 0$, Eq. (3.45) $\Leftrightarrow (|\nu|^3 - \beta) \leq 0$ and $|\nu| \leq 1/\beta$, i.e.,

$$|\nu| \leq \min\{\beta^{1/3}, 1/\beta\} = \begin{cases} 1 & \text{if } \beta = 1 \\ \beta^{1/3} < 1 & \text{if } 0 < \beta < 1 \\ 1/\beta < 1 & \text{if } \beta > 1 \end{cases} \quad (\nu \neq 0) \quad (3.46)$$

In turn, Eqs. (3.44) and (3.46) \Rightarrow

$$\epsilon = \beta |\nu| = \begin{cases} 1 & \text{if } \beta \geq 1 \\ \beta^{4/3} < 1 & \text{if } 0 < \beta < 1 \end{cases} \quad (\nu \neq 0) \quad (3.47)$$

Also, for the case $\eta = 1/2$, it has been shown that the stability conditions of the c - τ - η scheme is

$$f(\nu^2) \leq \tau \quad (\nu^2 \leq 2) \quad (3.48)$$

if $\nu^2 \leq 2$, where

$$f(s) \stackrel{\text{def}}{=} \frac{s(s+2)}{1+2s-s^2} \quad (0 \leq s \leq 2) \quad (3.49)$$

Note that (i)

$$1+2s-s^2 = -(s+\sqrt{2}-1)(s-\sqrt{2}-1) > 0 \quad \text{if } 0 \leq s \leq 2 \quad (3.50)$$

i.e., the denominator of the expression on the right side of Eq. (3.49) is not zero throughout the domain of $f(s)$ and therefore the function is well defined over its domain; and (ii)

$$\frac{df(s)}{ds} = \frac{2(2s^2+s+1)}{(1+2s-s^2)^2} > 0 \quad \text{if } 0 \leq s \leq 2 \quad (3.51)$$

i.e., $f(s)$ is monotonically increasing in its domain and therefore

$$0 = f(0) \leq f(s) \leq f(2) = 8 \quad (0 \leq s \leq 2) \quad (3.52)$$

The stability conditions of the $c\text{-}\tau\text{-}\eta$ scheme for the case $\eta = 1/2$ and $\nu^2 > 2$ can also be cast into an analytical form. However, the form is much more complicated and will not be presented here.

3.2. 2D and 3D extensions

For a 2D case using triangular meshes, or a 3D case using tetrahedral meshes, there is a natural extension of each of the 1D $a\text{-}\epsilon\text{-}\eta$ and $c\text{-}\tau\text{-}\eta$ schemes. As an example, consider Fig. 8 where the triangle $\triangle BDF$ and its three neighbors $\triangle BFH$, $\triangle BID$, and $\triangle DJF$ (which all lie on the $x\text{-}y$ plane) are shown. As explained in Sec. 2, each of the centroid mesh points G , A , C , and E shown in Fig. 3 is replaced in Fig. 8 by another associated interior point which is (i) defined by Eqs. (2.10) and (2.29) with $\zeta \geq 1$; and (ii) denoted by the same symbol and also marked by an open circle. The spatial solution point G' (also marked by a cross) associated with $\triangle BDF$ again is defined as the centroid of the hexagon $ABCDEF$. Other spatial solution points A' , C' , and E' are defined similarly. In addition, points K , L , and M (marked by triangles) depicted in Fig. 8, by definition, are the centroids of the quadrilaterals $GFAB$, $GBCD$, and $GDEF$, respectively.

Let each spatial solution point be assigned a unique identification index (an integer). As an example, let points G' , A' , C' , and E' be identified by the indices j , j_1 , j_2 , and j_3 , respectively. As such, as an example, the x - and y - coordinates of point G' will be denoted by x_j and y_j , respectively. Moreover, the space-time solution points (G', n) , (A', n) , (C', n) , and (E', n) , which lie on the n th time level and have the points G' , A' , C' , and E' being their spatial projections, respectively, will be denoted by (j, n) , (j_1, n) , (j_2, n) , and (j_3, n) , respectively. Also each space-time solution point (j, n) is associated with [13] (i) one SE denoted by $\text{SE}(j, n)$; and (ii) three BCEs denoted by $\text{CE}_{(k)}(j, n)$, $k = 1, 2, 3$, respectively, and a CCE which is the union of $\text{CE}_{(k)}(j, n)$, $k = 1, 2, 3$, and denoted by $\text{CE}(j, n)$. By definition, $\text{CE}_{(1)}(j, n)$ is the space-time cylinder sandwiched between the n th and $(n - 1/2)$ th time levels with the quadrilateral $GFAB$ being its spatial projection. $\text{CE}_{(2)}(j, n)$ and $\text{CE}_{(3)}(j, n)$ are defined identically except that the quadrilateral $GFAB$ are replaced by the quadrilaterals $GBCD$ and $GDEF$, respectively. It is seen that (i) the solution points (j, n) and (j_1, n) are the hosts of the space-time region occupied by $\text{CE}_{(1)}(j, n)$, (ii) the solution points (j, n) and (j_2, n) are the hosts of the space-time region occupied by $\text{CE}_{(2)}(j, n)$, and (iii) the solution points (j, n) and (j_3, n) are the hosts of the space-time region occupied by $\text{CE}_{(3)}(j, n)$,

Let the 2D counterpart of Eq. (1.1) be

$$\frac{\partial u}{\partial t} + a_x \frac{\partial u}{\partial x} + a_y \frac{\partial u}{\partial y} = 0 \quad (3.53)$$

where a_x , and a_y are constants. Then the 2D counterparts of Eqs. (1.4) and (1.6) are

$$\vec{h}^*(x, y, t; j, n) \stackrel{\text{def}}{=} [a_x u^*(x, y, t; j, n), a_y u^*(x, y, t; j, n), u^*(x, y, t; j, n)] \quad (3.54)$$

and

$$u^*(x, y, t; j, n) = u_j^n + (u_x)_j^n [(x - x_j) - a_x(t - t^n)] + (u_y)_j^n [(y - y_j) - a_y(t - t^n)] \quad (3.55)$$

respectively. Thus there are three independent marching variables, i.e., u_j^n , $(u_x)_j^n$, and $(u_y)_j^n$ associated with a space-time solution point (j, n) (i.e., point (G', n)).

Next let (i) (K, n) , (L, n) , and (M, n) denote the points on the n th time level with their spatial projections being points K , L , and M , respectively; (ii) the intermediate solution data stored at (j, n) , (j_1, n) , (j_2, n) , and (j_3, n) be evaluated from the given solution data at the $(n - 1/2)$ th time level using the 2D versions of the $a\text{-}\epsilon$ or $c\text{-}\tau$ scheme [7,13,31]; (iii) $[\hat{u}(K, n)]_j^n$ and $[\hat{u}(K, n)]_{j_1}^n$ denote the intermediate values of u at (K, n) evaluated using the intermediate solution data stored at the hosts (j, n) and (j_1, n) of $\text{CE}_{(1)}(j, n)$, respectively; (iv) $[\hat{u}(L, n)]_j^n$ and $[\hat{u}(L, n)]_{j_2}^n$ denote the intermediate values of u at (L, n) evaluated using the intermediate solution data stored at the hosts (j, n) and (j_2, n) of $\text{CE}_{(2)}(j, n)$, respectively; (v) $[\hat{u}(M, n)]_j^n$ and $[\hat{u}(M, n)]_{j_3}^n$ denote the intermediate values of u at (M, n) evaluated using the intermediate solution data stored at the hosts (j, n) and (j_3, n) of $\text{CE}_{(3)}(j, n)$, respectively; (vi) $[u(K, n)]_j^n$ and $[u(K, n)]_{j_1}^n$ denote the final values of u at (K, n) evaluated using the final solution data stored at the hosts (j, n) and (j_1, n) of $\text{CE}_{(1)}(j, n)$, respectively; (vii) $[u(L, n)]_j^n$ and $[u(L, n)]_{j_2}^n$ denote the final values of u at (L, n) evaluated using

the final solution data stored at the hosts (j, n) and (j_2, n) of $\text{CE}_{(2)}(j, n)$, respectively; and (viii) $[u(M, n)]_j^n$ and $[u(M, n)]_{j_3}^n$ denote the final values of u at (M, n) evaluated using the final solution data stored at the hosts (j, n) and (j_3, n) of $\text{CE}_{(3)}(j, n)$, respectively.

Moreover, for each $k = 1, 2, 3$, let (i) $A_k(j, n)$ denote the area of the spatial projection of $\text{CE}_{(k)}(j, n)$; (ii) $\hat{F}_k(j, n)$ denote the intermediate value of the flux of \vec{h}^* leaving $\text{CE}_{(k)}(j, n)$ through its top face evaluated using the intermediate solution data stored at the space-time solution point (j, n) ; (iii) $\hat{F}_k(j_k, n)$ denote the intermediate value of the flux of \vec{h}^* leaving $\text{CE}_{(k)}(j, n)$ through its top face evaluated using the intermediate solution data stored at the space-time solution point (j_k, n) ; (iv) $F_k(j, n)$ denote the final value of the flux of \vec{h}^* leaving $\text{CE}_{(k)}(j, n)$ through its top face evaluated using the final solution data stored at the space-time solution point (j, n) ; and (v) $F_k(j_k, n)$ denote the final value of the flux of \vec{h}^* leaving $\text{CE}_{(k)}(j, n)$ through its top face evaluated using the final solution data stored at the space-time solution point (j_k, n) . According to the above definitions, $A_1(j, n)$, $A_2(j, n)$, and $A_3(j, n)$ are the areas of the quadrilaterals $GFAB$, $GBCD$, and $GDEF$, respectively. Because these quadrilaterals are the spatial projections of $\text{CE}_{(k)}(j, n)$, $k = 1, 2, 3$, respectively, for each $k = 1, 2, 3$, $A_k(j, n)$ is the area of the top face of $\text{CE}_{(k)}(j, n)$.

With the aid of (i) the above definitions, (ii) the fact that point K depicted in Fig. 8 is the centroid of the quadrilateral $GFAB$ (i.e., the spatial projection of $\text{CE}_{(1)}(j, n)$), and (iii) Eq. (3.55) is a first-order Taylor's expansion, by using Eqs. (3.54) and (3.55), one can establish the following relations for several fluxes of \vec{h}^* leaving $\text{CE}_{(1)}(j, n)$ through its top face:

$$\hat{F}_1(j, n) = [\hat{u}(K, n)]_j^n A_1(j, n) \quad (3.56)$$

$$\hat{F}_1(j_1, n) = [\hat{u}(K, n)]_{j_1}^n A_1(j, n) \quad (3.57)$$

$$F_1(j, n) = [u(K, n)]_j^n A_1(j, n) \quad (3.58)$$

and

$$F_1(j_1, n) = [u(K, n)]_{j_1}^n A_1(j, n) \quad (3.59)$$

The current solution-coupling step will be constructed assuming the following dual-flux conservation relation:

$$F_1(j, n) + F_1(j_1, n) = \hat{F}_1(j, n) + \hat{F}_1(j_1, n) \quad (3.60)$$

By substituting Eqs. (3.56)–(3.59) into Eq. (3.60), one obtains

$$[u(K, n)]_j^n + [u(K, n)]_{j_1}^n = [\hat{u}(K, n)]_j^n + [\hat{u}(K, n)]_{j_1}^n \quad (3.61)$$

Similarly, by considering the fluxes at the top faces of $\text{CE}_{(2)}(j, n)$ and $\text{CE}_{(3)}(j, n)$ and imposing the dual-flux conservation relations similar to Eq. (3.60), one has

$$[u(L, n)]_j^n + [u(L, n)]_{j_2}^n = [\hat{u}(L, n)]_j^n + [\hat{u}(L, n)]_{j_2}^n \quad (3.62)$$

$$[u(M, n)]_j^n + [u(M, n)]_{j_3}^n = [\hat{u}(M, n)]_j^n + [\hat{u}(M, n)]_{j_3}^n \quad (3.63)$$

We assume the following weighted-averaging relations:

$$[u(K, n)]_j^n = (1 - \eta)[\hat{u}(K, n)]_j^n + \eta[\hat{u}(K, n)]_{j_1}^n \quad (3.64)$$

$$[u(L, n)]_j^n = (1 - \eta)[\hat{u}(L, n)]_j^n + \eta[\hat{u}(L, n)]_{j_2}^n \quad (3.65)$$

and

$$[u(M, n)]_j^n = (1 - \eta)[\hat{u}(M, n)]_j^n + \eta[\hat{u}(M, n)]_{j_3}^n \quad (3.66)$$

where η is a real adjustable parameter. In turn, by substituting Eqs. (3.64)–(3.66) into Eqs. (3.61)–(3.63), one has

$$[u(K, n)]_{j_1}^n = \eta [\hat{u}(K, n)]_j^n + (1 - \eta)[\hat{u}(K, n)]_{j_1}^n \quad (3.67)$$

$$[u(L, n)]_{j_2}^n = \eta [\hat{u}(L, n)]_j^n + (1 - \eta)[\hat{u}(L, n)]_{j_2}^n \quad (3.68)$$

and

$$[u(M, n)]_{j_3}^n = \eta [\hat{u}(M, n)]_j^n + (1 - \eta)[\hat{u}(M, n)]_{j_3}^n \quad (3.69)$$

respectively.

According to Eqs. (3.64)–(3.66), $[u(K, n)]_j^n$, $[u(L, n)]_j^n$ and $[u(M, n)]_j^n$ can be determined in terms of $[\hat{u}(K, n)]_j^n$, $[\hat{u}(K, n)]_{j_1}^n$, $[\hat{u}(L, n)]_j^n$, $[\hat{u}(L, n)]_{j_2}^n$, $[\hat{u}(M, n)]_j^n$, $[\hat{u}(M, n)]_{j_3}^n$, and a given value of η . On the other hand, because $t = t^n$ at points (j, n) , (K, n) , (L, n) , and (M, n) , Eq. (3.55) along with the definitions of $[u(K, n)]_j^n$, $[u(L, n)]_j^n$, and $[u(M, n)]_j^n$, \Rightarrow

$$u_j^n + (u_x)_j^n [x(K) - x_j] + (u_y)_j^n [y(K) - y_j] = [u(K, n)]_j^n \quad (3.70)$$

$$u_j^n + (u_x)_j^n [x(L) - x_j] + (u_y)_j^n [y(L) - y_j] = [u(L, n)]_j^n \quad (3.71)$$

and

$$u_j^n + (u_x)_j^n [x(M) - x_j] + (u_y)_j^n [y(M) - y_j] = [u(M, n)]_j^n \quad (3.72)$$

Here (i) $x(K)$ and $y(K)$ are the x - and y - coordinates of point K , (ii) $x(L)$ and $y(L)$ are the x - and y - coordinates of point L , and (iii) $x(M)$ and $y(M)$ are the x - and y - coordinates of point M .

Let

$$\det \begin{pmatrix} 1 & x(K) - x_j & y(K) - y_j \\ 1 & x(L) - x_j & y(L) - y_j \\ 1 & x(M) - x_j & y(M) - y_j \end{pmatrix} \equiv \det \begin{pmatrix} x(L) - x(K) & y(L) - y(K) \\ x(M) - x(K) & y(M) - y(K) \end{pmatrix} \neq 0 \quad (3.73)$$

i.e., points K , L , and M do not lie on a straight line. Then Eqs. (3.70)–(3.72) can be inverted and, as a result, u_j^n , $(u_x)_j^n$, and $(u_y)_j^n$ can be explicitly determined in terms of $[u(K, n)]_j^n$, $[u(L, n)]_j^n$, and $[u(M, n)]_j^n$ if the spatial coordinates of points (j, n) , K , L , and M are given. As such, given all the spatial geometric data, the final solution values at any (j, n) can be determined in terms of the given solution values at the $(n - 1/2)$ time level by using the 2D solution-coupling procedure describe above.

In a CESE 3D scheme using a spatial mesh constructed from tetrahedra, generally a solution point is associated with four independent mesh variables, four BCEs and one CCE. Also each BCE has two hosts. As such, construction of the 3D solution-coupling procedure is a straightforward extension of its 2D counterpart.

Finally, it should be emphasized that the use of a solution-coupling procedure generally will introduce numerical dissipation and, as a result, degrade accuracy. As such it is strongly recommended that, as long as it serves the purpose of preventing solution decoupling, this procedure should be applied as sparingly as possible, i.e., it should be used with a small value of η and/or applied once after a preset number of marching steps.

4. Conclusions and discussions

As a preliminary for the later development, a review of basic CESE ideas and schemes along with a discussion of several issues related to the application of the CESE method involving unstructured triangular/tetrahedral meshes was presented in Sec. 1. Among the issues discussed are: (A) geometric difficulties associated with a boundary which has high curvature or sharp corner and is also surrounded by triangular/tetrahedral meshes of extremely high aspect ratio, and (B) possible occurrences of solution decoupling in CESE simulations involving unstructured triangular/tetrahedral meshes.

To tackle the issue (A), Sec. 2 began by identifying the root cause of the geometry difficulty for the triangular-mesh case, i.e., the hexagon $ABCDEF$ depicted in Fig. 4 may become highly concave if (i) the

mesh points A , C , E , and G are designated, respectively, as the centroids of the associated triangles, and (ii) two neighboring triangles with high aspect ratio also have sharply different orientations. A rigorous mathematical analysis was then presented to validate the observation. According to this analysis, the centroid and in-center of a triangle are but two special cases with $\zeta = 0$ and $\zeta = 1$, respectively, of the family of the interior points defined by Eqs. (2.10), (2.29), and (2.32). By using the results presented in Eqs. (2.39)–(2.41), it becomes clear that, by replacing the centroid with another interior point with $\zeta \geq 1$, the hexagon $ABCDEF$ referred to above will become convex or much less concave. This conclusion has been verified by numerous numerical experiments. In fact, the geometric difficulty can be overcome by simply designating points A , C , E , and G (see Fig. 4), respectively, as the in-centers ($\zeta = 1$) of the associated triangles. Moreover, it was shown in Sec. 2 that the tetrahedral-mesh case can be dealt with in a completely parallel manner.

The new solution-coupling procedures described in Sec. 3 have become an integral part of the CESE code development. In fact, the nuisance of solution decoupling is avoided completely with the use of these new procedures.

References

1. S.C. Chang and W.M. To, *A New Numerical Framework for Solving Conservation Laws—The Method of Space-Time Conservation Element and Solution Element*, NASA TM 104495, August 1991.
2. S.C. Chang, On An Origin of Numerical Diffusion: Violation of Invariance under Space-Time Inversion, in *Proceedings, 23rd Conference on Modeling and simulation, April 30-May 1, 1992, Pittsburgh, PA, USA*, edited by W.G. Volt and M.H. Mickle, Part 5, p. 2727. Also published as NASA TM 105776.
3. S.C. Chang and W.M. To, A Brief Description of a New Numerical Framework for Solving Conservation Laws—The Method of Space-Time Conservation Element and Solution Element, in *Proceedings of the Thirteenth International Conference on Numerical Methods in Fluid Dynamics, Rome, Italy, 1992*, edited by M. Napolitano and F. Sabetta, Lecture Notes in Physics 414, (Springer-Verlag, New York/Berlin, 1992), p. 396.
4. S.C. Chang, *New Developments in the Method of Space-Time Conservation Element and Solution Element—Applications to the Euler and Navier-Stokes Equations*, NASA TM 106226.
5. S.C. Chang, The method of space-time conservation element and solution Element—A new approach for solving the Navier-Stokes and Euler equations, *J. Comput. Phys.*, **119**, 295 (1995).
6. S.T. Yu and S.C. Chang, *Treatments of Stiff Source Terms in Conservation Laws by the Method of Space-Time Conservation Element and Solution Element*, AIAA Paper 97-0435 (1997).
7. S.C. Chang, S.T. Yu, A. Himansu, X.Y. Wang, C.Y. Chow, and C.Y. Loh, The method of space-time conservation element and solution element—A new paradigm for numerical solution of conservation laws, in *Computational Fluid Dynamics Review 1998* edited by M.M. Hafez and K. Oshima (World Scientific, Singapore), Vol. 1, p. 206.
8. T. Molls and F. Molls, Space-Time Conservation Method Applied to Saint Venant Equations, *J. of Hydraulic Engr.*, **124(5)**, 501 (1998).
9. S.T. Yu, S.C. Chang, P.C.E. Jorgenson, S.J. Park and M.C. Lai, “Treating Stiff Source Terms in Conservation Laws by the Space-Time Conservation Element and Solution Element Method,” in *Proceedings of the 16th International Conference on Numerical Method in Fluid Dynamics, Arcachon, France, 6-10 July, 1998*, edited by C.H. Bruneau, (Springer-Verlag Berlin Heidelberg 1998), p. 433.
10. S.C. Chang, X.Y. Wang, and C.Y. Chow, *The Space-Time Conservation Element and Solution Element Method—A New High-Resolution and Genuinely Multidimensional Paradigm for Solving Conservation Laws. I. The Two-Dimensional Time Marching Schemes*, NASA TM—1998-208843, December, 1998.
11. S.C. Chang, X.Y. Wang, and C.Y. Chow, *The Space-Time Conservation Element and Solution Element Method—A New High-Resolution and Genuinely Multidimensional Paradigm for Solving Conservation Laws. II. Numerical Simulation of Shock Waves and Contact Discontinuities*, NASA TM—1998-208844, December, 1998.
12. S.C. Chang, X.Y. Wang, and C.Y. Chow, The space-time conservation element and solution element method: A new high-resolution and genuinely multidimensional paradigm for solving conservation laws, *J. Comput. Phys.*, **156**, 89 (1999).

13. X.Y. Wang, and S.C. Chang, A 2D non-splitting unstructured triangular mesh Euler solver based on the space-time conservation element and solution element method, *Computational Fluid Dynamics Journal*, **8(2)**, 309 (1999).
14. C. Zoppou and S. Roberts, Space-Time Conservation Method Applied to Saint Venant Equations: A Discussion, *J. of Hydraulic Engr.*, **125(8)**, 891 (1999).
15. N.S. Liu and K.H. Chen, *Flux: An Alternative Flow Solver for the National Combustion Code*, AIAA Paper 99-1079.
16. X.Y. Wang and S.C. Chang, A 3D structured/unstructured Euler solver based on the space-time conservation element and solution element method, in *A Collection of Technical Papers, 14th AIAA CFD Conference, June 28–July 1, 1999, Norfolk, Virginia*, AIAA Paper 99-3278.
17. S.C. Chang, X.Y. Wang and W.M. To, Application of the space-time conservation element and solution element method to one-dimensional convection-diffusion problems, *J. Comput. Phys.*, **165**, 189 (2000).
18. J. Qin, S.T. Yu, Z.C. Zhang, and M.C. Lai, Direct Calculations of Cavitating Flows by the Space-Time CESE Method, *J. Fuels & Lubricants, SAE Transc.*, **108(4)**, 1720 (2000).
19. C.Y. Loh, L.S. Hultgren and S.C. Chang, Wave computation in compressible flow using the space-time conservation element and solution element method, *AIAA J.*, **39(5)**, 794 (2001).
20. Z.C. Zhang, S.T. Yu, and S.C. Chang, A Space-Time Conservation Element and Solution Element Method for Solving the Two- and Three-Dimensional Unsteady Euler Equations Using Quadrilateral and Hexahedral Meshes, *J. Comput. Phys.*, **175**, 168 (2002).
21. K.B.M.Q. Zaman, M.D. Dahl, T.J. Bencic, and C.Y. Loh, Investigation of A ‘Transonic Resonance’ with Convergent-Divergent Nozzles, *J. Fluid Mech.*, **463**, 313 (2002).
22. C.Y. Loh and K.B.M.Q. Zaman, Numerical Investigation of ‘Transonic Resonance’ with A Convergent-Divergent Nozzle, *AIAA J.*, **40(12)**, 2393 (2002).
23. S. Motz, A. Mitrovic, and E.-D. Gilles, Comparison of Numerical Methods for the Simulation of Dispersed Phase Systems, *Chemical Engineering Science*, **57**, 4329 (2002).
24. S. Cioc and T.G. Keith, Application of the CESE Method to One-Dimensional Flow in Fluid Film Bearings, *STLE Tribology Transactions*, **45**, 167 (2002).
25. S.C. Chang, *Courant Number Insensitive CESE Schemes*, AIAA Paper 2002-3890 (2002).
26. S. Cioc and T.G. Keith, Application of the CESE Method to Two-Dimensional Flow in Fluid Film Bearings, *International J. of Numer. Methods for Heat & Fluid Flow*, **13(2)**, 216 (2003).
27. S. Cioc, F. Dimofte, T.G. Keith, and D.P. Fleming, Computation of Pressurized Gas Bearings Using the CESE Method, *STLE Tribology Transactions*, **46(1)**, 128 (2003).
28. S. Cioc, F. Dimofte, and T.G. Keith, Application of the CESE Method to Wave Journal Bearings, *STLE Tribology Transactions*, **46(2)**, 179 (2003).
29. A. Ayasoufi and T.G. Keith, Application of the Conservation Element and Solution Element Method in Numerical Modeling of Heat Conduction with Melting and/or Freezing, *International J. of Numer. Methods for Heat & Fluid Flow*, **13(4)**, 448 (2003).
30. I.S. Chang, *Unsteady Underexpanded Jet Flows*, AIAA Paper 2003-3885.
31. S.C. Chang and X.Y. Wang, *Multidimensional Courant Number Insensitive CESE Euler Solvers for Applications Involving Highly Nonuniform Meshes*, AIAA Paper 2003-5280.
32. A. Ayasoufi and T.G. Keith, Application of the Conservation Element and Solution Element Method in Numerical Modeling of Axisymmetric Heat Conduction with Melting and/or Freezing, *JSME International J. Series B*, **47(1)**, 115 (2004).
33. A. Ayasoufi and T.G. Keith, Application of the Conservation Element and Solution Element Method in Numerical Modeling of Three-dimensional Heat Conduction with Melting and/or Freezing, *Transactions of the ASME, J. of Heat Transfer*, **126(6)**, 937 (2004).
34. Y.I. Lim, S.C. Chang, and S.B. Jorgensen, A Novel Partial Differential Algebraic Equation (PDAE) Solver: Iterative Space-Time Conservation Element/Solution Element (CESE) Method, *Computers and Chemical Engineering*, **28**, 1309 (2004)

35. Y.I. Lim and S.B. Jorgensen, A Fast and Accurate Numerical Method for Solving Simulated Moving Bed (SMB) Chromatographic Separation Problems, *Chemical Engineering Science*, **59**, 1931 (2004).
36. Y.I. Lim, An Optimization Strategy for Nonlinear Simulated Moving Bed Chromatography: Multi-level Optimization Procedure (MLOP), *Korea J. Chem. Eng.*, 21(4), 836 (2004).
37. C.K. Kim, S.T. John Yu, and Z.C. Zhang, Cavity Flow in Scramjet Engine by the Space-Time Conservation Element and Solution Element Method, *AIAA J.*, **42(5)**, 912 (2004).
38. M. Zhang, S.T. John Yu, S.C. Lin, S.C. Chang, and I. Blankson, Solving Magnetohydrodynamic Equations Without Special Treatment for Divergence-Free Magnetic Field, *AIAA J.*, **42(12)**, 2605 (2004).
39. K.S. Im, M.C. Lai, S.T. John Yu, and Robert R. Matheson, Jr., Simulation of Spray Transfer Process in Electrostatic Rotary Bell Sprayer, *ASME J. of Fluid Engineering*, **126(3)**, 449 (2004).
40. S. Jerez, J.V. Romero, and M.D. Rosello, A Semi-Implicit Space-Time CESE Method to Improve Mass Conservation through Tapered Ducts in Internal Combustion Engines, *Math. and Computer Modeling*, **40**, 941 (2004).
41. B.S. Venkatachari, G.C. Cheng, and S.C. Chang, *Development of A Transient Viscous Flow Solver Based on Conservation Element-Solution Element Framework*, AIAA Paper 2004-3413.
42. S.C. Chang, Y. Wu, V. Yang, and X.Y. Wang, Local Time Stepping Procedures for the Space-Time Conservation Element and Solution Element Method, *International J. Comput. Fluid Dynamics*, **19(5)**, 359 (2005).
43. Y.I. Lim, S.B. Jorgensen, and I.H. Kim, Computer-Aided Model Analysis for Ionic Strength-Dependent Effective Charge of Protein in Ion-Exchange Chromatography, *Bio-Chem. Eng. J.*, **25(2)**, 125 (2005).
44. T.I. Tseng and R.J. Yang, Simulation of the Mach Reflection in Supersonic Flows by the CESE Method, *Shock Waves*, **14(4)**, 307 (2005).
45. B. Wang, H. He, and S.-T.J. Yu, Direct Calculation of Wave Implosion for Detonation Initiation, *AIAA J.*, **43(10)**, 2157 (2005).
46. S.C. Chang, *Explicit von Neumann Stability Conditions for the c - τ Scheme—A Basic Scheme in the Development of the CESE Courant Number Insensitive Schemes*, NASA TM 2005-213627, April 2005.
47. J.C. Yen and D.A. Wagner, *Computational Aeroacoustics Using a Simplified Courant Number Insensitive CESE Method*, AIAA Paper 2005-2820.
48. I.S. Chang, C.L. Chang, and S.C. Chang, *Unsteady Navier-Stokes Rocket Nozzle Flows*, AIAA Paper 2005-4353.
49. S.C. Chang, *Courant Number and Mach Number Insensitive CESE Euler Solvers*, AIAA Paper 2005-4355
50. S.C. Chang, A. Himansu, C.Y. Loh, X.Y. Wang, and S.T. Yu, Robust and Simple Non-Reflecting Boundary Conditions for the Euler Equations—A New Approach Based on the Space-Time CESE Method, in *Proceedings, NSF-CBMS Regional Research Conference on Mathematical Methods in Nonlinear Wave Propagation, North Carolina A&T State University, Greensboro, North Carolina, May 15-19, 2002*, edited by D.P. Clemence and G. Tang, p. 155-190, Vol. 379 in *Contemporary Mathematics*, American Mathematical Society (2005). Also published as NASA/TM-2003-212495/Rev1.
51. B.S. Venkatachari, G.C. Cheng, and S.C. Chang, *Courant Number Insensitive Transient Viscous Flow Solver Based on CESE Framework*, AIAA Paper 2005-00931.
52. T.I. Tseng and R.J. Yang, Numerical Simulation of Vorticity Production in Shock Diffraction, *AIAA J.*, **44(5)**, 1040 (2006).
53. M. Zhang, S.-T. Yu, S.C.H. Lin, S.C. Chang, and I. Blankson, Solving the MHD Equations By the Space-Time Conservation Element and Solution Element Method, *J. Comput. Phys.*, **214**, 599 (2006).
54. I.S. Chang, C.L. Chang, and S.C. Chang, *3D Unsteady Navier-Stokes Rocket Nozzle Flows*, AIAA Paper 2006-4775.
55. C.L. Chang, *Time-accurate, Unstructured-Mesh Navier-Stokes Computations with the Space-time CESE Method*, AIAA Paper 2006-4780.
56. S.C. Chang, *On Space-Time Inversion Invariance and Its Relation to Non-Dissipativeness of a CESE Core Scheme*, AIAA Paper 2006-4779. Also published as NASA TM 2006-214385.

57. X. Feng, Y. Zhou, and S.T. Wu, A Novel Numerical Implementation for Solar Wind Modeling by the Modified Conservation Element/Solution Element Method, *Astrophys. J.*, **655**(1), 1110 (2007).
58. C.L. Chang, *Three-Dimensional Navier-Stokes Calculations Using the Modified Space-Time CESE Method*, AIAA Paper 2007-5818.
59. S.C. Chang, *The $a(3)$ Scheme—A Fourth-Order Neutrally Stable CESE Solver*, AIAA Paper 2007-4321.
60. S.C. Chang, *The $a(4)$ Scheme—A High-Order Neutrally Stable CESE Solver*, AIAA Paper 2007-5820.
61. S.C. Chang, *The $a(3)$ Scheme—A Fourth-Order Space-Time Flux-Conserving and Neutrally Stable CESE Solver* (A revised and expanded version of AIAA Paper 2007-4321), NASA TM 2008-215138, April 2008.
62. C.-L. Chang and M. Choudhari, “Hypersonic Viscous Flow over Large Roughness Elements,” AIAA Paper 2009-0173, to appear in Theoretical and Computational Fluid Dynamics Journal, special issue on Global Instability of Complex Flows.
63. S.C. Chang, “A New Approach for Constructing Highly Stable High Order CESE Schemes,” AIAA Paper 2010-543. Also appear as NASA/TM-2010-216777.
64. C.-L. Chang, M. Choudhari and F. Li, “Numerical Computations of Hypersonic Boundary Layers over Surface Irregularities,” AIAA Paper 2010-1572, 2010.
65. G.C. Cheng, B. Venkatachari, C.-L. Chang and S.C. Chang, “The Space-Time CESE Method for High-Fidelity Flow Simulations,” presented at Parallel CFD 2010 Conference, Kaohsiung, Taiwan, May 2010.
66. J.C. Yen, A.B. Kimbrell and C.H. Connor, “Study of WICS Data Using an Emerging Lower-Order CAA Method,” AIAA Paper 2010-1742.
67. A.B. Kimbrell, J.C. Yen and C.H. Connor, “CAA Study of WICS Data Using JUSTUS,” presented in 2010 Aircraft-Stores Compatibility Symposium sponsored by International Test and Evaluation Association.
68. Y.Y. Chen, L. Yang and S.T. John Yu, Simulation of Waves in Elastic solids of Cubic Symmetry by the Conservation Element and Solution Element Method, *Wave Motion*, in press.
69. L. Yang, Y.Y. Chen and S.T. John Yu, Velocity-Stress Equations for Waves in Solids of Hexagonal Symmetry Solved by the Space-Time CESE Method, *ASME J. of Vibration and Acoustics*, in press.
70. Other CESE references are posted on: <http://www.grc.nasa.gov/www/microbus>.
71. R.A. Horn and C.R. Johnson, *Matrix Analysis*, Cambridge University Press, 1985.
72. To be presented in a NASA Technical Memorandum.

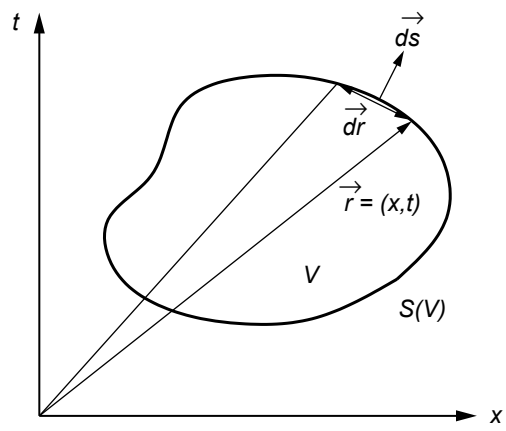
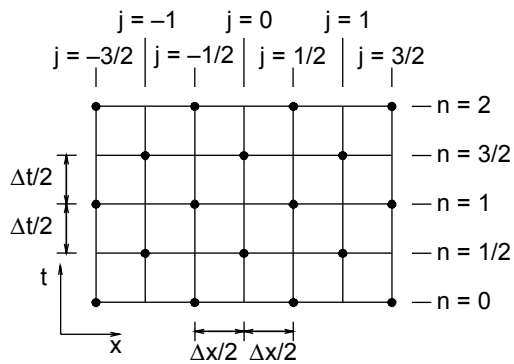
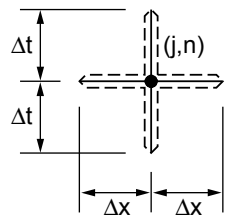


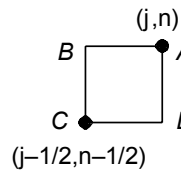
Figure 1.—A surface element on the boundary $S(V)$ of an arbitrary space-time volume V .



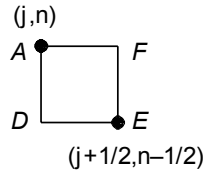
2(a)—The space-time mesh.



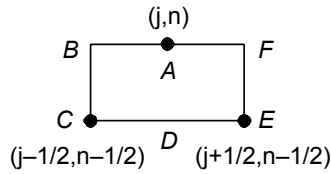
2(b) SE(j,n).



2(c) CE₋(j,n).



2(d) CE₊(j,n).



2(e) CE(j,n)

Figure 2.—The SEs and CEs.

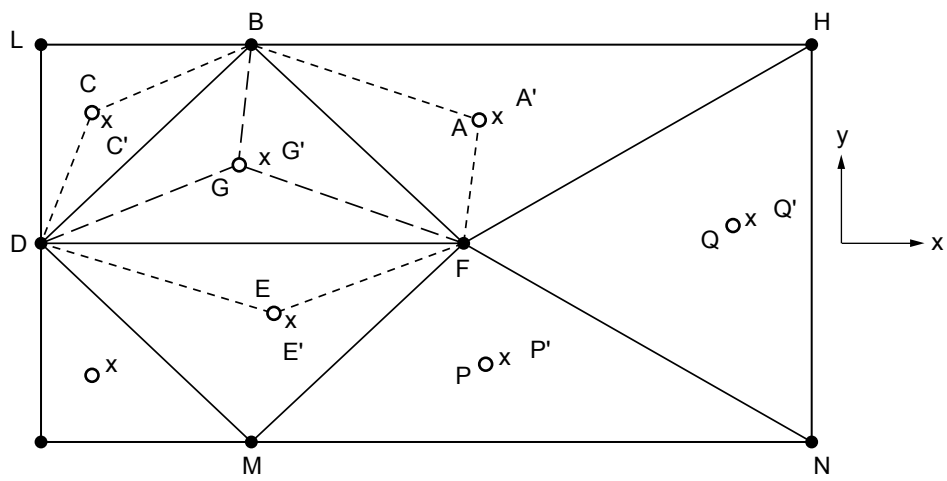


Figure 3.—A spatial domain formed by triangles.

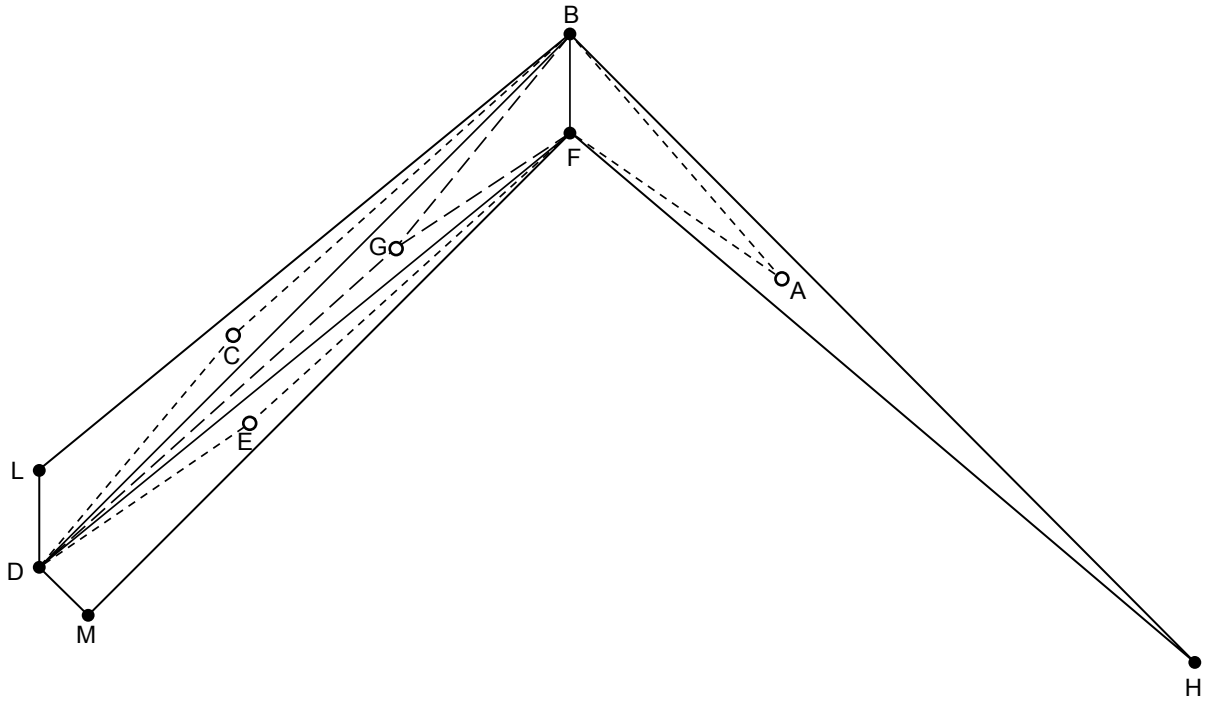


Figure 4.—Neighboring triangles with high aspect ratios and sharply different orientations.

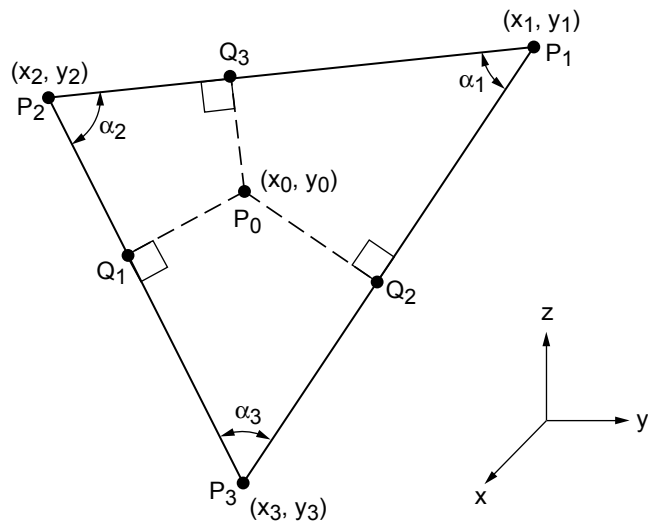
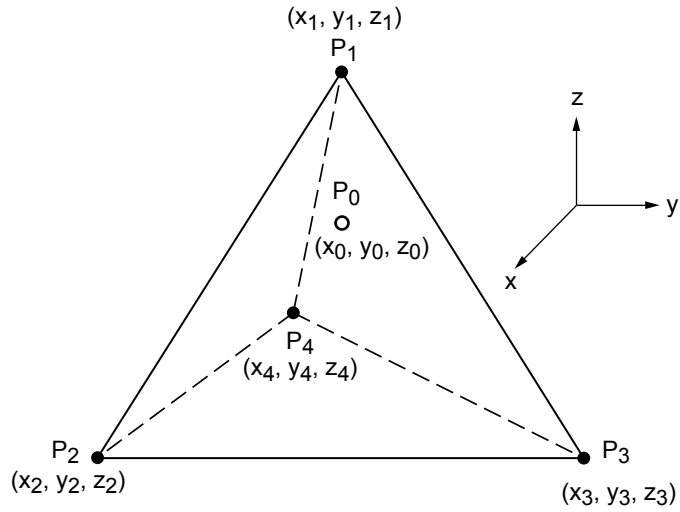
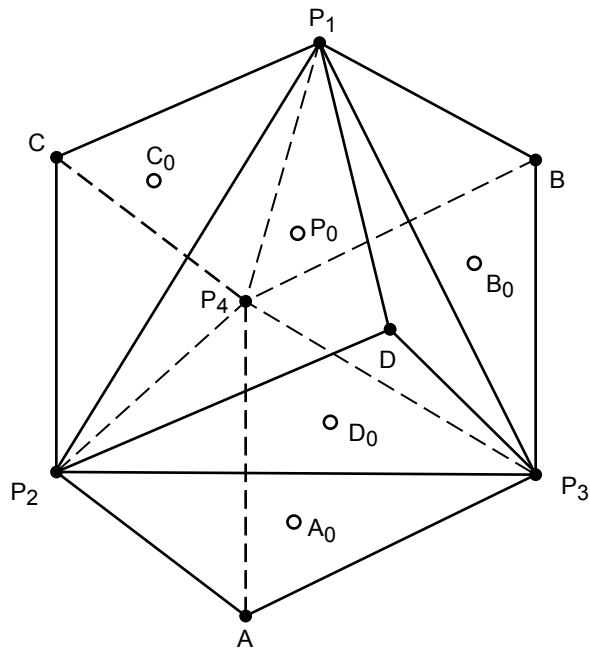


Figure 5.—The perpendicular projections of point P_0 on the three sides (or their extensions) of a triangle $\Delta P_1, P_2, P_3$.



6(a).—A tetrahedron $P_1 P_2 P_3 P_4$ and a point P_0 .



6(b).—A tetrahedron and four neighboring tetrahedra.

Figure 6.—Five neighboring tetrahedra in the x - y - z space.

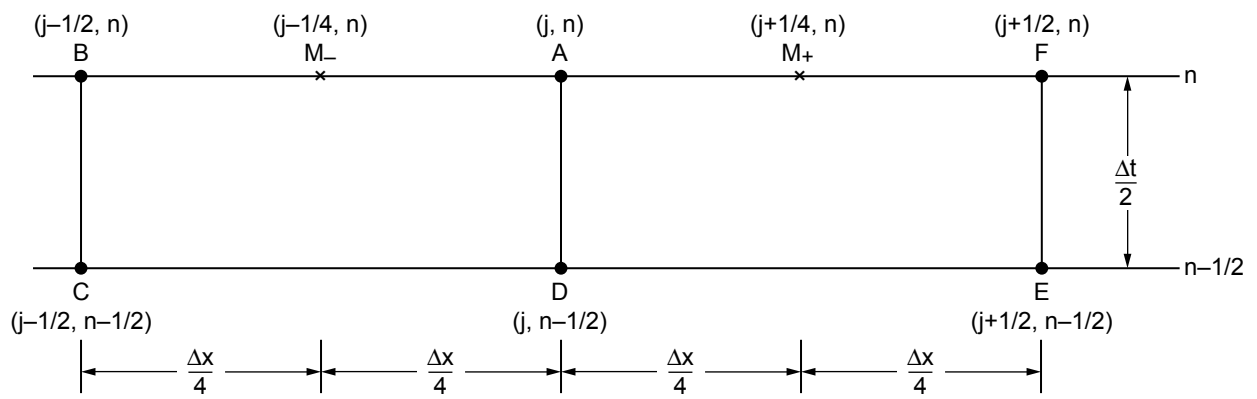


Figure 7.—Construction of the $a-\epsilon-\eta$ and $c-\tau-\eta$ schemes.

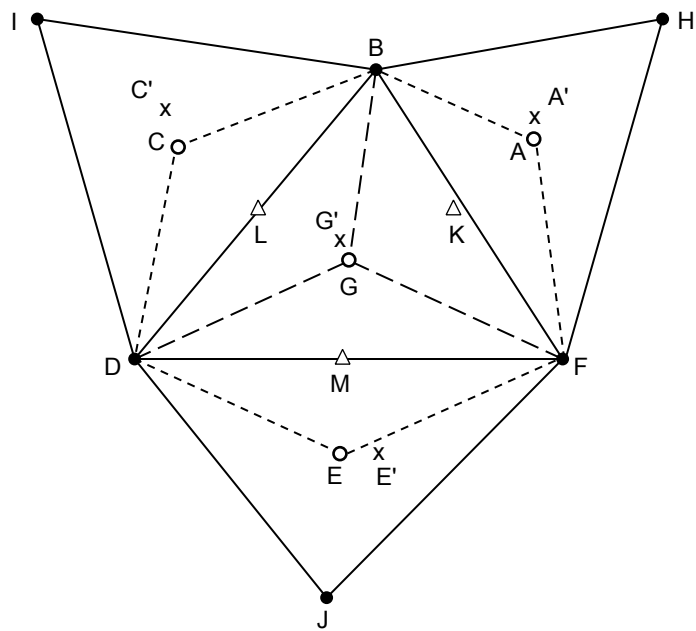


Figure 8.—Construction of the 2D a-ε-η and c-τ-η schemes.

REPORT DOCUMENTATION PAGE			Form Approved OMB No. 0704-0188		
<p>The public reporting burden for this collection of information is estimated to average 1 hour per response, including the time for reviewing instructions, searching existing data sources, gathering and maintaining the data needed, and completing and reviewing the collection of information. Send comments regarding this burden estimate or any other aspect of this collection of information, including suggestions for reducing this burden, to Department of Defense, Washington Headquarters Services, Directorate for Information Operations and Reports (0704-0188), 1215 Jefferson Davis Highway, Suite 1204, Arlington, VA 22202-4302. Respondents should be aware that notwithstanding any other provision of law, no person shall be subject to any penalty for failing to comply with a collection of information if it does not display a currently valid OMB control number.</p> <p>PLEASE DO NOT RETURN YOUR FORM TO THE ABOVE ADDRESS.</p>					
1. REPORT DATE (DD-MM-YYYY) 01-09-2013		2. REPORT TYPE Technical Memorandum		3. DATES COVERED (From - To)	
4. TITLE AND SUBTITLE Recent Development in the CESE Method for the Solution of the Navier-Stokes Equations Using Unstructured Triangular or Tetrahedral Meshes With High Aspect Ratio			5a. CONTRACT NUMBER		
			5b. GRANT NUMBER		
			5c. PROGRAM ELEMENT NUMBER		
6. AUTHOR(S) Chang, Sin-Chung; Chang, Chau-Lyan; Yen, Joseph, C.			5d. PROJECT NUMBER		
			5e. TASK NUMBER		
			5f. WORK UNIT NUMBER WBS 599489.02.07.03.04.13.01		
7. PERFORMING ORGANIZATION NAME(S) AND ADDRESS(ES) National Aeronautics and Space Administration John H. Glenn Research Center at Lewis Field Cleveland, Ohio 44135-3191			8. PERFORMING ORGANIZATION REPORT NUMBER E-18704		
9. SPONSORING/MONITORING AGENCY NAME(S) AND ADDRESS(ES) National Aeronautics and Space Administration Washington, DC 20546-0001			10. SPONSORING/MONITOR'S ACRONYM(S) NASA		
			11. SPONSORING/MONITORING REPORT NUMBER NASA/TM-2013-218061		
12. DISTRIBUTION/AVAILABILITY STATEMENT Unclassified-Unlimited Subject Categories: 34 and 64 Available electronically at http://www.sti.nasa.gov This publication is available from the NASA Center for AeroSpace Information, 443-757-5802					
13. SUPPLEMENTARY NOTES					
14. ABSTRACT In the multidimensional CESE development, triangles and tetrahedra turn out to be the most natural building blocks for 2D and 3D spatial meshes. As such the CESE method is compatible with the simplest unstructured meshes and thus can be easily applied to solve problems with complex geometries. However, because the method uses space-time staggered stencils, solution decoupling may become a real nuisance in applications involving unstructured meshes. In this paper we will describe a simple and general remedy which, according to numerical experiments, has removed any possibility of solution decoupling. Moreover, in a real-world viscous flow simulation near a solid wall, one often encounters a case where a boundary with high curvature or sharp corner is surrounded by triangular/tetrahedral meshes of extremely high aspect ratio (up to 10^6). For such an extreme case, the spatial projection of a space-time compounded conservation element constructed using the original CESE design may become highly concave and thus its centroid (referred to as a spatial solution point) may lie far outside of the spatial projection. It could even be embedded beyond a solid wall boundary and causes serious numerical difficulties. In this paper we will also present a new procedure for constructing conservation elements and solution elements which effectively overcomes the difficulties associated with the original design. Another difficulty issue which was addressed more recently is the well-known fact that accuracy of gradient computations involving triangular/tetrahedral grids deteriorates rapidly as the aspect ratio of grid cells increases. The root cause of this difficulty was clearly identified and several remedies to overcome it were found through a rigorous mathematical analysis. However, because of the length of the current paper and the complexity of mathematics involved, this new work will be presented in another paper.					
15. SUBJECT TERMS The space-time CESE method; Computational fluid dynamics; Numerical analysis					
16. SECURITY CLASSIFICATION OF:			17. LIMITATION OF ABSTRACT UU	18. NUMBER OF PAGES 48	19a. NAME OF RESPONSIBLE PERSON STI Help Desk (email: help@sti.nasa.gov)
a. REPORT U	b. ABSTRACT U	c. THIS PAGE U			19b. TELEPHONE NUMBER (include area code) 443-757-5802

